(12) INTERNATIONAL APPLICATION PUBLISHED UNDER THE PATENT COOPERATION TREATY (PCT)

(19) World Intellectual Property Organization
International Bureau

(43) International Publication Date
9 March 2017 (09.03.2017)

WIPO | PCT

(10) International Publication Number
WO 2017/035559 A1

(51) International Patent Classification:
*B01F 11/02* (2006.01) *B01J 19/10* (2006.01)
*B01F 13/00* (2006.01)

(21) International Application Number:
PCT/AU2016/000299

(22) International Filing Date:
30 August 2016 (30.08.2016)

(25) Filing Language: English

(26) Publication Language: English

(30) Priority Data:
2015903626 4 September 2015 (04.09.2015) AU

(71) Applicant: **MONASH UNIVERSITY** [AU/AU]; Wellington Road, Clayton, Victoria 3800 (AU).

(72) Inventors: **ALAN, Tuncay**; 7D/12 Marine Parade, St Kilda VIC 3182 (AU). **NEILD, Adrian**; 15 Lambert Road, Toorak, VIC 3142 (AU). **PHAN, Hoang van**; 8 Michael Court, Springvale North VIC 3171 (AU). **COSKUN, M Bulut**; 3/131 Clayton Road, Oakleigh East VIC 3166 (AU). **NGUYEN, Hoai An Le**; LH314 Logan Hall, 28 Sports Walk, Monash University 3800 VIC (AU).

(74) Agent: **SMOORENBURG PATENT & TRADE MARK ATTORNEYS**; PO Box 515, Ringwood VIC 3134 (AU).

(81) Designated States *(unless otherwise indicated, for every kind of national protection available)*: AE, AG, AL, AM, AO, AT, AU, AZ, BA, BB, BG, BH, BN, BR, BW, BY, BZ, CA, CH, CL, CN, CO, CR, CU, CZ, DE, DK, DM, DO, DZ, EC, EE, EG, ES, FI, GB, GD, GE, GH, GM, GT, HN, HR, HU, ID, IL, IN, IR, IS, JP, KE, KG, KN, KP, KR, KZ, LA, LC, LK, LR, LS, LU, LY, MA, MD, ME, MG, MK, MN, MW, MX, MY, MZ, NA, NG, NI, NO, NZ, OM, PA, PE, PG, PH, PL, PT, QA, RO, RS, RU, RW, SA, SC, SD, SE, SG, SK, SL, SM, ST, SV, SY, TH, TJ, TM, TN, TR, TT, TZ, UA, UG, US, UZ, VC, VN, ZA, ZM, ZW.

(84) Designated States *(unless otherwise indicated, for every kind of regional protection available)*: ARIPO (BW, GH, GM, KE, LR, LS, MW, MZ, NA, RW, SD, SL, ST, SZ, TZ, UG, ZM, ZW), Eurasian (AM, AZ, BY, KG, KZ, RU, TJ, TM), European (AL, AT, BE, BG, CH, CY, CZ, DE, DK, EE, ES, FI, FR, GB, GR, HR, HU, IE, IS, IT, LT, LU, LV, MC, MK, MT, NL, NO, PL, PT, RO, RS, SE, SI, SK, SM, TR), OAPI (BF, BJ, CF, CG, CI, CM, GA, GN, GQ, GW, KM, ML, MR, NE, SN, TD, TG).

**Published**:

— *with international search report (Art. 21(3))*

WO 2017/035559 A1

(54) Title: MEMBRANE AND METHOD FOR MICROMIXING

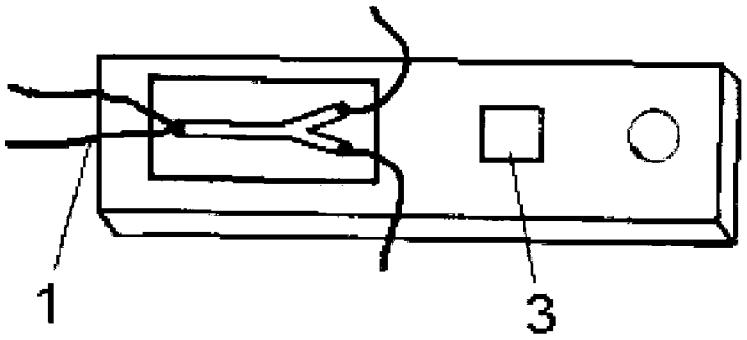



FIG. 1a

(57) Abstract: The present invention relates to a membrane and method for microfluidic mixing, the membrane having an upper membrane surface and a lower membrane surface and comprising at least one discontinuity. A composite may be formed by combination of two or more of the membranes. In a preferred embodiment the membrane generates a vortical acoustic streaming field when subjected to acoustic excitations. In one embodiment the method of mixing has efficiency of >80%, preferably >90% in 3 ms at a fluid flow rate of 60 µl/min.

# MEMBRANE AND METHOD FOR MICROMIXING

## FIELD OF INVENTION

[0001] The present invention relates to the field of acoustic mixers.

[0002] In one form the invention relates to an acoustic mixer comprising a microfabricated silicon nitride membrane.

[0003] In one particular aspect the present invention is suitable for use as a mixer for extremely fast and homogeneous mixing.

[0004] It will be convenient to hereinafter describe the invention in relation to microfluidic mixing however it should be appreciated that the present invention is not limited to that use only and has a number of applications including nano-dispersal.

## BACKGROUND ART

[0005] It is to be appreciated that any discussion of documents, devices, acts or knowledge in this specification is included to explain the context of the present invention. Further, the discussion throughout this specification comes about due to the realisation of the inventor and/or the identification of certain related art problems by the inventor. Moreover, any discussion of material such as documents, devices, acts or knowledge in this specification is included to explain the context of the invention in terms of the inventor's knowledge and experience and, accordingly, any such discussion should not be taken as an admission that any of the material forms part of the prior art base or the common general knowledge in the relevant art in Australia, or elsewhere, on or before the priority date of the disclosure and claims herein.

[0006] Efficient, homogeneous mixing of fluids is crucial for a variety of microfluidic applications ranging from complex chemical reactions[1] and protein studies[2] to nanoparticle synthesis[3–5]. However, fluid flows at micro and nano scales usually lie in the laminar

regime, which is characterised by a low Reynolds number ($Re = \rho UL/\mu \ll 100$, where $\rho$ is the fluid density, $U$ is the flow velocity, $L$ is the characteristic length and $\mu$ is the fluid's dynamic viscosity). Consequently, in the absence of external influences, mixing at this scale is dominated by diffusion, a prohibitively long process. [6]

[0007] To simultaneously reduce the mixing time and increase the mixing efficiency (i.e. how homogeneously fluids are mixed) in microfluidic channels, many enhancement strategies have been investigated. Broadly, they can be divided into two categories: passive[7–11] and active methods.[12–17]. Each group has its own advantages and limitations in terms of effectiveness, mixing time, control and ease of operation. Since passive mixers (such as the chaotic mixer[8] and the hydrodynamic focusing mixer[7]) do not require any external devices nor a power source, they are extremely simple to operate and integrate with different applications. However, they are usually outperformed by their active counterparts with respect to mixing efficiency and time[18,19]. Furthermore, the required channel length of passive mixers can compromise the appealing compactness of microfluidic systems.

[0008] Acoustic mixers offer significant advantages for rapid mixing. Firstly, they do not impose any limitations on the working fluid medium such as conductivity[14] or requirement of magnetic particle suspensions[15]. Secondly, acoustic energy can safely be used in various biological and chemical applications. Thirdly, acoustofluidics is a strong, mature and thriving field with many demonstrated capabilities such as particle manipulation[20–26] and, of course, mixing[13,27–33].

[0009] An acoustic mixer's operation depends on the resonance of vibrating features to perturb the steady flow to induce mixing. A compelling example of this approach is an air bubble trapped in a microfluidic channel[13,29]. The actuation of a microbubble results in a streaming field in the form of vortices due to the oscillatory boundary. Compared to pressure fluctuations from other types of ultrasonic transducers, these vortices disturb the flow more strongly[34,35] and rapidly. (In comparison, the fluids need to travel for more than 4mm to be mixed completely using integrated digital transducers[31].) Nevertheless, the primary control parameter of a bubble mixer is its radius, thus even a slight disturbance to

the bubble's shape can affect the resonant frequency[32]. Furthermore, bubble instability can arise from changes in flow pressure and heating. Oscillating sharp-edges can overcome the bubble instability problem in exchange for weaker flow disturbances[32].

## SUMMARY OF INVENTION

[0010] An object of the present invention is to provide an improved membrane suitable for use in an acoustic mixer.

[0011] A further object of the present invention is to provide an improved design of acoustic mixer that provides easy control.

[0012] Yet another object of the present invention is to provide an acoustic mixer that generates significant disturbance and a well-defined stable frequency.

[0013] It is another object of the embodiments described herein to overcome or alleviate at least one of the above noted drawbacks of related art systems or to at least provide a useful alternative to related art systems.

[0014] In a first aspect of embodiments described herein there is provided a membrane for microfluidic mixing, having an upper membrane surface and a lower membrane surface and comprising at least one discontinuity.

[0015] Typically, the discontinuity is a hole or aperture in boundary conditions of said membrane and located between said upper membrane surface and lower membrane surface.

[0016] Typically, the membrane comprises micro-fabricated silicon nitride or silicon.

[0017] The discontinuity may be defined by a periphery of various geometries including polygonal shapes (particularly square, rectangular or star shapes) and closed symmetric curves (particularly circular shapes). The membrane may also comprise more than one

discontinuity.

[0018] In a preferred embodiment the membrane of the present invention generates a vortical acoustic streaming field when subjected to acoustic excitations. The membrane may for example, exhibit transverse vibrations when subjected to acoustic excitations. Furthermore, the vortical acoustic streaming field may comprise vortices having a plane perpendicular to the direction of the transverse vibrations of the membrane.

[0019] In another embodiment of the present invention there is provided an acoustic mixer having a membrane, the membrane surface comprising at least one discontinuity. A mixer of this type is useful for a number of applications including rapid mixing of fluids, or nano-dispersal.

[0020] In another embodiment of the present invention there is provided a composite membrane for microfluidic mixing comprising two or more membranes, each membrane having a membrane surface comprising at least one discontinuity.

[0021] In another embodiment of the present invention there is provided a microfluidic chip comprising a membrane having a surface comprising at least one discontinuity and a piezoelectric disk for applying acoustic excitation to the membrane.

[0022] There is further provided a method of mixing comprising the steps of:

(i) immersing the membrane in a fluid, and

(ii) applying acoustic excitation to the fluid such that the membrane exhibits transverse vibrations and a streaming field in the form of vortices is generated.

[0023] In one embodiment the method of mixing has efficiency of >80%, preferably >90% in 3 ms at a fluid flow rate of 60 µl/min.

[0024] In another embodiment the method of mixing is >80%, preferably >86% in 4 ms

at a fluid flow rate of 60 µl/min.

[0025] In a further embodiment, the present invention provides a method of manufacturing the membrane of the present invention, the method comprising the steps of:

(i) coating an upper surface of a silicon wafer with a photoresistant substance,

(ii) carrying out photolithography to expose a predetermined peripheral shape of a discontinuity on the upper surface,

(iii) etching the exposed shape to create the discontinuity in the form of a hole defined by the discontinuity and extending from the upper surface to a lower surface of the silicon wafer, and

(iv) removing the photoresistant substance from the silicon wafer.

[0026] Other aspects and preferred forms are disclosed in the specification and/or defined in the appended claims, forming a part of the description of the invention.

[0027] In essence, embodiments of the present invention stem from the realization that when a membrane comprising a discontinuity is immersed in fluid and subjected to acoustic excitation, a strong streaming field in the form of vortices may be generated, the vortices tending to centre at the discontinuity, and thus has a critical role it has on the streaming field. Hence the presence of the hole can increase the volume force responsible for driving the streaming field. Furthermore it has been realised that this effect on the streaming field can be harnessed for applications such as acoustic mixing.

[0028] Advantages provided by the present invention comprise the following:

- the membrane can be used to provide an improved design of acoustic mixer;

- the membrane can be used to provide an acoustic mixer that generates

significant disturbance and a well-defined stable frequency.

[0029] Further scope of applicability of embodiments of the present invention will become apparent from the detailed description given hereinafter. However, it should be understood that the detailed description and specific examples, while indicating preferred embodiments of the invention, are given by way of illustration only, since various changes and modifications within the spirit and scope of the disclosure herein will become apparent to those skilled in the art from this detailed description.

## BRIEF DESCRIPTION OF THE DRAWINGS

[0030] Further disclosure, objects, advantages and aspects of preferred and other embodiments of the present application may be better understood by those skilled in the relevant art by reference to the following description of embodiments taken in conjunction with the accompanying drawings, which are given by way of illustration only, and thus are not limitative of the disclosure herein, and in which:

FIG. 1 is an illustration of a microfluidic device according to the present invention.

FIG. 1(a) is a photograph of the microfluidic device showing the bottom outlet (1), piezo disk on a Si substrate (3).

FIG. 1(b) is a schematic of the acoustic membrane mixer (where *W* and *H* denote the PDMS channel's width and height.)

FIG. 1(c) is a cross-sectional plan of the membrane together with the bottom outlet. (where *a*, *d* and *h* denote the membrane's side length, hole size and thickness respectively.)

FIG. 1(d) is a simplified side view of the microfluidic device, showing how the bottom outlet (1) is placed beneath the SiN chip. Layers shown are PDMS channel (5), SiN chip (7), epoxy (9) and glass slide (11).

FIG. 1(e) illustrates one embodiment of a fabrication process of the SiN chip and the PDMS channel comprising the following steps: (i) a silicon wafer is coated on both surfaces with silicon nitride; (ii) part of the silicon nitride is etched from one surface; (iii) part of the silicon nitride layer is etched from the other surface; (iv). the silicon layer is etched anisotropically at 54.7° from the (100) (i.e. horizontal) plane releasing the membrane; (v) a silicon wafer undergoes DRIE Etch to form the desired shape; (vi) PDMS is cast onto the etched surface of the silicon wafer; (vii) the PDMS layer is peeled off the wafer; and (viii) the PDMS layer is plasma bonded to the silicon nitride membrane.

FIG. 2 illustrates mixing characteristics observed using the membrane of the present invention.

FIG. 2(a) is an example of the location chosen for intensity analysis and the transition length for mixing time calculation and indicates the mixed region (12), unmixed region (13) and transition length (14).

FIG. 2(b) shows edge detection using MATLAB's built-in function edge with 'Canny' option. FIG. 2(c) is a graph illustrating raw intensity (arbitrary units) of the mixed (21) and unmixed region (22). FIG. 2(d) is a graph illustrating normalised intensity (to range between 0 and 1, using raw data (24)) of the transition length, the fitted step function 925) and the identified mixing transition length ($L_{mix,}$ 23). All x-axes are in pixels. For this example, *MI* = 0.92 and $t_{mix}$ = 25 ms

FIG. 3 illustrates the boundary conditions for the two types of membrane as set in COMSOL.

FIG. 3(a) shows the mechanical BC and FIG. 3(b) shows the thermal BC of the continuous including areas of symmetry (26), no slip (27), isothermal (28), velocity (29), no stress (30), none (31) .

FIG. 3(c) and FIG. 3(d) show the mechanical and thermal BC of the membrane with

the hole. The bold black lines represent the membrane. The "Velocity" mechanical BC is set according to Eq. (10c). The channel's dimensions are $W$ = 750 $\mu$m and $H$ = 70 $\mu$m, the membrane's dimensions $a$ = 420 $\mu$m and $d$ = 100 $\mu$m.

FIG. 4 illustrates COMSOL simulation results.

FIG. 4(a) shows the mesh convergence parameter (lower is better) with an example mesh generated at $\delta_{th}/d_{mesh}$ = 0.1 with $u_1$ (40), $v_1$ (41), $p_1$ (42) and $T_1$ (43).

FIG. 4(b) is a surface plot of the first-order pressure field.

FIG. 4(c) is a surface plot of the magnitude and the normalised arrow plot of **v**1.

FIG. 4(d) is a plot of the components of $V_1$ (45) and $U_1$ (46) along the dashed lines arrows located at the midpoint of the membrane's surface.

FIG. 4(e) is a surface plot of the body force magnitude and the field's normalised arrow plots created by the membrane with and without the hole, respectively. The dashed lines in Fig. 4(d) indicate the viscous boundary layer. The plots in FIGS. 4(b)-4(e) are produced at $\delta_{th}/d_{mesh}$ = 2. The fine mesh at the hole's edge shown in the inset in (a) is kept unchanged for all $\delta_{th}/d_{mesh}$ ratio.

FIG. 5 illustrates flow visualisation and mixing of the acoustic membrane at 10 microlitres/min.

FIG. 5(a) is a streaming pattern at 224 kHz (indicating the assumed mixing transition length (50)).

FIG. 5(b) illustrates mixing at 187 kHz.

FIG. 5(c) is a streaming pattern at 235 kHz.

FIG. 5(d) is a schematic of the resultant vortices around the membrane.

FIG. 5(e) illustrates mixing of a membrane with a rectangular hole at 137 kHz.

FIG. 5(f) illustrates mixing of a membrane with two square holes at 146 kHz.

FIG. 5(g) illustrates mixing with a membrane with a hole offset from the centre at 228 kHz.

FIG. 5(h) and FIG. 5(i) show the case when fluid flows through the membrane's hole when it is turned OFF and ON, respectively, at 136 kHz. The membrane in FIG. 5(a), FIG. 5(b) and FIG. 5(c) has a = 455 mm and d = 200 mm; the membrane used in (g) has a = 425 mm and d = 120 mm; and the one in FIG. 5(h) and FIG. 5(i) has a = 230 mm and d = 100 mm. All scale bars are 1000 mm unless otherwise specified.

FIG. 6 illustrates the mixing characterisation of the membranes with circular holes.

FIG. 6(a) and FIG. 6(b) show the mixing index and mixing time for various geometry ratios a=d at different Peclet numbers Pe, respectively. Mixing with the membrane with no hole (a=d) is performed in a 750-mm-wide channel at Q = 2 and 10 microlitres/min, and its corresponding mixing time is not shown in FIG. 6(b). H and N markers represent the experiments with channel's width W = 750 and 1000 mm, respectively. The arrow indicates the best circular mixer: a=d = 2:275, MI = 0:90 and $t_{mix}$ = 3 ms. Errors are estimated by one standard error. Legend: w/d=2.300=164.5 kHz (90), w/d=2.275=187 kHz (91), w/d=4.250=165 kHz (92), w/d=5.250=161 kHz (93), w/d=3.667=150 kHz (94); w/d=3.500=122kHz (95)

FIG. 7 illustrates the mixing characterisation of the membranes with different hole geometries.

FIG. 7(a) and FIG. 7(b) show the mixing index and mixing time for a square hole and multiple holes at different Pecket numbers Pe (136 kHz (80), 137 kHz (81); 146 kHz

(82); (122.5 kHz (84); 144k Hz (85)). The device uses the same membrane with two circular holes, except that the holes are covered by air bubbles instead of being completely immersed. This bubble device is tested at Q = 5;10;15 and 20 microlitres/min. H and N markers represent the experiments with channel's width W = 750 and 1000 mm, respectively. The arrow indicates the best mixer in this case, the double square holes membrane, which can achieve MI = 0:86 and $t_{mix}$ = 4 ms. Errors are estimated by one standard error.

FIG. 8 illustrates how different streaming patterns observed when the holes are covered by air bubbles in a 1000-mm-wide channel.

FIG. 8(a) and FIG. 8(b) show mixing of a fully immersed membrane with double circular holes at 10 microlitres/min and 122.5 kHz (including unmixed (70) and mixed regions (71) and transition length (73)).

FIG. 8(c) is a visualisation of the flow caused by the immersed membrane 10 microlitres/min and 107.7 kHz.

FIG. 8(d), FIG. 8(e) and FIG. 8(f) show mixing performance and flow visualisation of the bubble membrane at 5 microlitres/min and 144 kHz. For the immersed membrane: MI = 0:81 and tmix = 26:4 ms; for the bubble membrane: MI = 0:78 and tmix = 47:3 ms. All x and y coordinates in FIGS. 8(a)-(e) are in pixels.

FIG. 9 illustrates composite membranes according to the present invention. The geometric properties of the membranes having been modified to enable high throughput operation and efficient mixing.

FIG. 9(a) is a schematic drawing of a resonator comprising four identical membranes showing a view of the (i) top face, (ii) bottom face, (iii) perspective, (iv) cross section, and (v) detail at the cross section along H-H 100:1 scale to illustrate the variable thickness.

FIG. 9(b) is a schematic drawing of a resonator comprising eight identical membranes which have optimized geometric properties in combination to provide a high throughput mixer, the schematic showing a view of the (i) op face, (ii) bottom face, (iii) perspective, (iv) cross section, and (v) detail at the cross section along A-A 100:1 scale to illustrate the variable thickness.

FIG. 9(c) is a schematic drawing of a multi-layer stack of two resonator each comprising eight identical membranes. The multi-layer assembly results in a significant increase in throughput and enhances mixing efficiency, the schematic showing a view of the (i) top face, (ii) perspective, and (iii) cross section of the device along B-B of Fig. 9(c)(1).

FIG. 10 illustrates two liquids co-flowing through the composite membrane depicted at FIG. 9(b).

FIG. 10a shows two liquids co-flowing at a total flow rate of 5 ml/min.

FIG. 10b shows two liquids instantaneously mixing at 1.3MHz operation.

FIG. 10c shows two liquids co-flowing at a total flow rate of 10 ml/min.

FIG. 10d shows two liquids instantaneously mixing at 1.07MHz operation.

FIG. 11 illustrates a method of fabricating membranes according to the present invention in 5 steps: (i) a double sided polished wafer of silicon is spin-coated with a 30 micrometer thick SU-8 3025 coating of photoresist; (ii) star shaped patterns are exposed via photolithography; (iii) DRIE Etch 600 cycles are carried out using a standard Bosch process; (iv) the etch is continued for another 50-100 cycles until the membranes are fully released; and (v) the photoresist coating is removed to reveal the finished membrane according to the present invention.

FIG. 12 illustrates a device according to the present invention.

FIG. 12(a) is an isometric view of the device.

FIG. 12(b) is a schematic view of the flow setup with arrows indicating direction of solvent flow (75), direction of antisolvent flow (76) and direction of mixed solution flow (77).

## DETAILED DESCRIPTION

[0031] In a particularly preferred embodiment, the present invention is utilised as an acoustic membrane, preferably a silicon nitride (SiN) membranes containing specially designed microfabricated features for efficient mixing. The system uses robust microfabricated structures with precisely defined geometries to generate a highly controllable streaming field. Under acoustic excitations, the membrane generates a vortical acoustic streaming field that is inherently different from that of a bubble: the vortices' plane is perpendicular to the direction of the membrane's transverse vibrations and the contingent presence of the hole. In contrast to a continuous membrane without a hole, these steady streaming fields are significantly stronger, leading to extremely good mixing performance comparable to that of a bubble mixer, but with the added advantage of precise control throughout operation.

[0032] The complexity of the observed vortices points to an intricate fluid-structure interaction. Without wishing to be bound by theory it is hypothesised that the hole's presence gives rise to a discontinuity to the otherwise continuous boundary conditions on the membrane surface. The following Experimental section includes numerical simulations that show how the body force field, which is responsible for inducing streaming, changes with the inclusion of the hole.

[0033] The Experimental section also illustrates the mixing performance at different flow rates for various geometries such as holes having a circular, square and rectangular shaped periphery. Most notably, rapid, homogeneous mixing is possible with 90% mixing efficiency at 60 $\mu$l/min total flow rate (Peclet number $\approx$ 8333 $\pm$ 3.5%) with 3 ms mixing time. Various geometries of the holes have also been tested, and it was observed that a membrane with a

couple of square holes can mix fluid at 4 ms and 86% efficiency at $Pe \approx 8333 \pm 3.5\%$. Additionally, investigations on the effects of having the holes covered by air bubbles yield interesting results. The streaming pattern is markedly different: the bubbles do not couple with each other as observed in the case of an immersed membrane, i.e. fluid only flows through the vortices generated by one bubble, reducing the mixing performance. A mixer according to the present invention is a potential candidate for microfluidic applications that require mixing such as nanoparticles synthesis.

[0034] Furthermore, a membrane with two circular holes which are covered by air bubbles is compared to when the membrane is fully immersed. It was found that coupling between the vortices of the holes occurs only when membrane is immersed; while with the bubble membrane, the upstream vortices of the holes can act as a blockage to fluid flow passing it.

## METHODOLOGY

### Fabrication and experimental set-up

[0035] The experimental device comprised a Y-shaped microfluidic channel made from polydimethyl siloxane (PDMS) bonded on a SiN chip containing the membranes (FIG. 1(a)). The fabrication processes for both the membrane and the channel are summarised in FIG. 1(e). For the membranes, firstly, the backside openings and front-side geometric features were patterned on 1-$\mu$m-thick SiN coated (100)-oriented Si wafers (4D LABS, Canada) through photolithography and reactive ion etching (RIE). The wafers are then immersed in a 5M KOH solution at 65°C for approximately 15 hours to selectively etch the Si and release the SiN membranes. The wafers were then scribed into small chips, each containing a 1-$\mu$m-thick SiN membrane with width $a$ ranging from 210 to 475 $\mu$m. Importantly, the membranes contained through holes of varying shapes, with characteristic lengths denoted by $d$. The membrane fabrication steps were inspired by similar designs employed in specialised transmission electron microscopy (TEM) grids[36–38].

[0036] The PDMS channels were fabricated using standard procedures. The features

were patterned on a (100) Si wafer, which is then etched by deep reactive ion etching (DRIE). The surface was rendered hydrophobic by a layer of teflon coating. PDMS was mixed with curing agent (SYLGARD® 184, Dow Corning) at ratio 10:1 w/w, and then cast on the mould. The mixture was left in a vacuum pump for 2 hours, and then on a hot plate at 65°C for complete curing. Finally, the PDMS channel was peeled off, cut and bonded onto the chip containing the membranes. The channel width $W$ ranged from 750 to 1000 $\mu$m, and the height $H$ varied between 70 to 86 $\mu$m.

[0037] After assembly, the entire structure was adhered together with the bottom outlet (Cole-Parmer® thin wall tubing) to a glass slide using epoxy (Selleys® Araldite). The device was excited by a piezoelectric disk (Ferroperm Piezoceramics), which was also bonded on the glass slide with epoxy. To initialise the system, water was pumped through the channel while ensuring that it also exited through the bottom outlet (the membrane was completely immersed). After this step, the outlet was blocked so that the fluid only flowed over the membrane.

[0038] Water with and without fluorescent dye (Invitrogen™Molecular Probes™) was injected into each of the two inlets by means of a syringe pump (kdScientific KDS-101-CE). The flow rates of both streams were kept equal, and their total flow rate $Q$ was chosen to be 10, 20, 40, 60 and 80 $\mu$l/min unless otherwise stated. The PZT was driven by a signal generator (Stanford Research Systems DS345) and an amplifier (T&C Power Conversion, Inc. AG 1006) at 200 $V_{pp}$. The membrane's resonant frequency was found experimentally by frequency sweeping. Flow visualisation was performed with 2.01 $\mu$m fluorescent particles (Bangs Laboratories, Inc.™) suspended in a water solution with 2 wt% PEG (CAS: 9003-11-6, Sigma-Aldrich). All experiments were recorded by a PixeLINK camera at 15 frames per second.

**Data analysis**

[0039] The effects of varying the total flow rate and different PDMS channel's dimensions were captured by the dimensionless Peclet number $Pe$:

$$Pe = \frac{UL}{D} \qquad (1)$$

where $U$ is the average flow velocity, $L$ the characteristic length and $D$ the diffusion coefficient of the fluorescent dye. ( $D = 1.5 \times 10^{-3}$ m$^2$/s was used in the calculations[39].)

[0040] Next, to quantify how good mixing was the fluorescence intensity of the recorded videos was analysed. After each frame was converted into grayscale (and rotated as necessary to ensure that the channel was horizontal), the channel walls were identified using MATLAB's built-in edge detection function 'edge'. The mixed and unmixed regions were chosen randomly downstream and upstream respectively (FIG. 2a), from which the intensities were obtained. An example of this choice and the edge detection image are shown in FIG. 2(a) and (b), and the corresponding intensity in grayscale is given in FIG. 2(c). The intensities were then used to calculate the mixing index $MI$:[40]

$$MI = 1 - \frac{\sqrt{\frac{1}{N}\sum_{i=1}^{N}(I_i - \bar{I})}}{\sqrt{\frac{1}{N}\sum_{i=1}^{N}(I_i' - \bar{I}')}}. \qquad (2)$$

where $N$ is the number of pixels of each region, $I_i$ and $\bar{I}$ denotes the local raw intensity of the *i-th* pixel and the average raw intensity of the mixed region respectively, and $()'$ denotes the intensity of the unmixed region. ($MI$ being closer to 1 implies mixing is more uniform.) This particular formula for $MI$ was chosen among the others as it was shown to be the least affected by lighting conditions and microscopes. [40]

[0041] In addition to homogeneity, the speed of mixing the fluids was determined. The mixing time $t_{mix}$ was estimated by the common methods reported in literature for acoustic mixers: [29,30,32]

$$t_{mix} = L_{mix}/U \qquad (3)$$

where $L_{mix}$ is the calculated mixing length based on the assumed transition length and $U = Q/WH$ is the average flow velocity in the channel. Faster mixing time has important implications in applications of micro fluidic mixing, such as higher monodispersity for synthesis of lipid nanoparticles[4]. To approximate $L_{mix}$, firstly, a step function in the form of $y = C_1 + C_2/(1 + e^{-C3(x-C4)})$,where $C_i$ are constant coefficients, was fitted to the normalised intensity of the chosen transition length. The cut-off intensities were equal to 2% of the maximum value of the fitted curve above and below the minimum and maximum of said curve, respectively. These two values dictate $L_{mix}$ in pixels, which is then converted into $\mu$m by scaling it with the channel's width.

[0042] To quantify the uncertainty in the analysis process, data across 15 frames (i.e. one full second in real-time) was analysed and averaged. The error bar was estimated by one standard error of these 15 data sets.

**Numerical simulation**

[0043] Without wishing to be bound by theory, it was hypothesised that firstly, a continuous (i.e. holeless) membrane can generate a streaming field, albeit a weak one, as is the case for a vibrating bubble or a flexural plate wave[41]. Secondly, is was assumed that the hole introduces a discontinuity to the boundary conditions at its perimeter, leading to a higher velocity gradient, especially within the Stokes' boundary layer. And finally, it is assumed that this gradient results in a strong volume force field that is responsible for the observed microstreaming vortices. The hypothesis is supported by numerical simulations and experimental results.

[0044] Specifically, it can be assumed that a fluid volume that is being disturbed by vibrating structures/surfaces (for example, a vibrating air/water interface). Applying the perturbation method on the fluid's pressure field, $p$, the velocity field, $\mathbf{v}$, and the fluid's density, $\rho$, yields:

$$p = p_0 + \varepsilon p1 + \varepsilon^2 p_2 \qquad (4a)$$

$$\mathbf{v} = \mathbf{v}_0 + \varepsilon\mathbf{v}_1 + \varepsilon^2\mathbf{v}_2 \qquad (4b)$$

$$\rho = \rho_0 + \varepsilon\rho_1 \qquad (4c)$$

where $\varepsilon$ is a small perturbation and subscripts 0, 1 and 2 denote the unperturbed, first-order and second-order value, respectively. The acoustic streaming (steady microstreaming) pattern that is experimentally observed is the time-averaged second-order velocity field: $\mathbf{v}_s = \langle \mathbf{v}_2 \rangle$.

[0045] There are generally two ways to find $\mathbf{v}_s$: (i) the time-dependent Navier-Stokes equation can be solved while forcing the velocity field at the membrane surface to be equal to the membrane's vibration, or (ii) the first-order velocity field had to be found to calculate the body force $\mathbf{F}$ that drives the streaming field:[42,43]

$$\mathbf{F} = -\rho_0\langle(\mathbf{v}_1 \nabla)\mathbf{v}_1 + \mathbf{v}_1(\nabla \mathbf{v}_1)\rangle \qquad (5)$$

[0046] The force field is then used as the input to the steady-state compressible Navier-Stokes equation (with appropriate boundary conditions):

$$\rho_0(\mathbf{v}_s \nabla)\mathbf{v}_s = -\nabla p_2 + \mu\nabla^2\mathbf{v}_s + (\mu_B + \tfrac{1}{3}\mu)\nabla(\nabla \mathbf{v}_s) + \mathbf{F} \qquad (6)$$

where $\mu$ and $\mu_B$ is the dynamic and bulk viscosity of fluid, respectively.

[0047] The first-order velocity field $\mathbf{v}_1$ itself can be obtained by two methods:

1. The first-order pressure field $p_1$ is found from the viscous Helmholtz equation. Then, $\mathbf{v}_1$ is calculated as $\mathbf{v}_1 = -\nabla p_1/i\omega\rho$ ($\omega$: excitation angular frequency, $\rho$: fluid's density, and $i$: the imaginary unit). [44]

2. $\mathbf{v}_1$ can be solved directly from the perturbation equations for the thermoacoustics fields.[45,46]

[0048] Importantly, if one employs method 1, the body force **F** must be corrected by an exponential decay function[42,44]. This is necessary to take into account the effects of the no-slip condition at the walls and the viscous boundary layer (Stokes' layer), the thickness of which is given by:

$$\delta = \sqrt{\frac{2\mu}{\omega\rho_0}} \qquad (7)$$

where $\omega$ is the excitation angular frequency. At a typical excitation frequency of 150 kHz, $\delta$ = 1.378 $\mu$m.

[0049] Computationally, solving the time-dependent Navier-Stokes equations is more time-consuming than the method of calculating the body force from the first-order velocity field. This is because once $\mathbf{v}_1$ is obtained, only the stationary Navier-Stokes equation need be solved. And even for finding $\mathbf{v}_1$, approach 1 (solving the Helmholtz equations) is significantly more computationally efficient because it need only solve for one variable, the pressure field, and gives a reasonably accurate approximation provided that the correct decay function is chosen.

[0050] The right decay function can prove challenging to find, especially for the cases with complicated geometries such as the singularity at the through hole's edges. The thermoacoustics approach, on the other hand, allows for the correct body force to be calculated directly from $\mathbf{v}_1$ without needing any modifications, regardless of the geometry. The downside is that it is more computationally expensive than method 1: the unknown variables are both $p_1$ and $\mathbf{v}_1$, plus the first-order temperature field $T_1$:

$$T = T_0 + \varepsilon T_1 + \varepsilon^2 T_2 \qquad (8)$$

[0051] The thermoacoustics equations also involves an important parameter, the thermal boundary layer thickness:

$$\delta_{th} = \sqrt{\frac{2D_{th}}{\omega}} \tag{9}$$

where $D_{th}$ is fluid's thermal diffusivity. At 150 kHz, $\delta_{th}$ = 0.551 $\mu$m. The temperature field changes rapidly within this thermal boundary layer.

[0052] In this study, method 2 (solving the thermoacoustics equations) is chosen to model the membrane. COMSOL Multiphysics 5.0 is used to solve for the first-order fields ($p_1$, $\mathbf{v}_1$, and $T_1$) with its Thermoacoustics Module. Only the 2D cross-section of the channel and the membrane is simulated. (Reasons for only performing a 2D simulation are discussed later.) All water's properties used in the model are given in the ESI.

[0053] To show that the presence of the hole can significantly enhance mixing, modeling was carried out for both a 420-$\mu$m-wide membrane with and without a 100-$\mu$m-diameter circular hole. The boundary conditions (BC) are:

$$T_1 = 0, \text{ on all walls} \tag{10a}$$

$$\mathbf{v}_1 = \mathbf{0}, \text{ on all walls, except} \tag{10b}$$

$$\mathbf{v}_1 = 0\mathbf{e}_x + U_0 w(x)\mathbf{e}_y, \text{ on membrane's surface} \tag{10c}$$

where $U_0$ is the velocity amplitude, $w(x)$ is the membrane's deflection shape, $\mathbf{e}_x$ and $\mathbf{e}_y$ are the unit vectors in $x$ and $y$-directions respectively. The mechanical BCs and device dimensions are given in FIG. 3 (see the last picture in FIG. 1(e) to visualise the modeled cross-section). To reduce the memory requirement, the symmetry of the system is utilised, the pressure and velocity fields are computed segregated from the temperature field, and the fluid in the cavity below the membrane is truncated at 150 $\mu$m (instead of having the full 500-$\mu$m-high cavity with a "No-slip" condition at the bottom wall) by the "No stress" condition implemented by COMSOL:

$$\left[-p_1\mathbf{I}+\mu\left(\nabla\mathbf{v}_1+(\nabla\mathbf{v}_1)^T\right)-\left(\frac{2}{3}\mu-\mu_B\right)(\nabla\cdot\mathbf{v}_1)\mathbf{I}\right]\mathbf{n}=0 \qquad (11)$$

where $\mathbf{I}$ is the identity matrix, $\mathbf{n}$ is the outward pointing surface normal vector, and $(\ )^T$ denotes the matrix transpose operator. This condition forces the total surface stress to be zero. (The isothermal condition need not be set on this wall.)

[0054] With regards to the "Velocity" BC, it is first necessary to find the deflection shape $w(x)$. For simplicity, it was assumed that $w(x)$ is equal to the fundamental resonance mode shape. For a holeless membrane, the fixed-fixed beam solution applies:[47]

$$w(x) = \cos k_1(x/a - 0.5) + C\cosh k_1(x/a - 0.5) \qquad (12)$$

where $k_1 \approx 4.730$, $C = \sin(k_1/2)/\sinh(k_1/2)$ and $a$ is the membrane side length. For the membrane with hole, the first mode shape is calculated using COMSOL's Plate Physics Module, and a 4th-order polynomial is fitted on the obtained deflection. For the modelled membrane ($a$ = 420 $\mu$m and $d$ = 100 $\mu$m):

$$w(xr) \approx 1.529x'^4 - 5.213x'^3 + 6.318'^2 + 8.034 \times 10^{-4}x' \qquad (13)$$

where $x'=x/\frac{a-d}{2}\left(0 \le x \le \frac{a-d}{2}\right)$ is the normalised distance from the fixed edge. (The polynomial has $R^2 \approx 1$.)

[0055] The velocity amplitude $U0$ is set such that:

$$\int_0^a U_0 w(x)\,\mathrm{d}x = a_0\omega a \qquad (14)$$

where $a_0$ is the scaling excitation amplitude (arbitrarily chosen to be 1 nm in the simulations).

[0056] Because of the small geometry at the hole's edge, a mesh convergence analysis is performed on $p_1$, $\mathbf{v}_1$ and $T_1$ to ensure the validity of the results. The maximum mesh size in the fluid bulk is set to be 10 times as large as that at the domain's walls: $d_{bulk} = 10d_{mesh}$. The mesh size is varied by changing the ratio $\delta_{th}/d_{mesh}$ from 0.25 to 2.75. (The thermal boundary layer thickness is used to scale the mesh because it is the smallest value compared to the viscous layer thickness and the membrane thickness.) The mesh convergence is quantified by the relative convergence parameter $C(g)$[46]:

$$C(g) = \sqrt{\frac{\int (g - g_{\text{ref}})^2 \, dx\,dy}{\int (g_{\text{ref}})^2 \, dx\,dy}} \tag{15}$$

[0057] Where $g$ is the solution for a particular mesh size and $g_{ref}$ is the reference solution. The lower $C(g)$ is, the more "converged" the mesh size is. The reference value was chosen as $\delta_{th}/d_{mesh} = 3$, which results in $\approx 1.52 \times 10^6$ degrees of freedom (dofs) and uses up to 10.50GB of RAM.

[0058] The physics of the membrane obviously presents a complicated fluid-structure interaction problem. Continuous membrane structures have previously been studied experimentally and theoretically for their applications in fluid pumping,[41,48] and the membrane-fluid coupling effect has been investigated[49]. However, the presence of the through-hole (not considered in the earlier studies) substantially complicates the problem: fluid loading and damping on both sides of the membrane can change its vibration mode, the fluid on each side can couple to each other, and there is a very strong acoustic streaming, a nonlinear effect.

[0059] As a result of the system's complexity, some assumptions were made about the numerical model. Firstly, the coupling between the fluid motion and the vibration of the membrane was neglected. Secondly, a 3D model was needed to find the actual streaming field: it is experimentally observed to be parallel to the membrane's surface (i.e. perpendicular to the membrane's transverse vibration). It is not justifiable to find the streaming pattern from a 2D simulation, as it would imply the streaming is on the plane

normal to the membrane's surface. Unfortunately, a 3D model is too costly: the need to include the cavity beneath the membrane would significantly increase the already high number of dofs to be solved. For reference, a 3D symmetrical model of a holeless membrane with $\delta_{th}/d_{mesh}$ = 0.1 has ≈ 10 × $10^6$ dofs. Thus, in this study, only a two-dimensional approximation that the body force driving the streaming field is substantially stronger with the presence of the hole is dealt with.

## RESULTS

### Numerical results

[0060] As a first step in the numerical study, a mesh convergence analysis was performed (FIG. 4(a)). Since only the body force is of interest, a maximum mesh size of $\delta_{th}/d_{mesh}$ = 2 at the walls is sufficiently accurate (all variables have achieved $10^{-4}$ convergence threshold, except the temperature variation $T_1$ which has achieved $C(g)$ = $10^{-3}$). It is noteworthy that to avoid numerical singularities, the edges at the hole are filleted, and the mesh size there is always kept constant.

[0061] FIG. 4(b)-(d) show the pressure field $p_1$ and velocity field $\mathbf{v}_1$ (see ESI for the temperature distribution $T_1$). Simulations show that the presence of the hole results in a significant increase in the body force (FIG. 4(e) and (f)). The membrane with through hole can generate a body force of 8.5 × $10^4$ N/m$^3$, as opposed to an approximate 7 × $10^2$ N/m$^3$ force without it. For comparison, the gravity body force is close to 1 × $10^4$ N/m$^3$.

[0062] This jump of 2 orders of magnitude supports the hypothesis that the hole's presence both enhances and complicates the streaming effect. Moreover, the volume force is expected to be concentrated around the edge of the hole (FIG. 4(e)) instead of being spread out along the membrane's surface (FIG. 4(f)). It is only possible to show the expected increase in strength of the streaming vortices associated with the hole because the vortice patterns are not modeled. (Nevertheless, all experiments confirm that the vortices always centre around the hole for different hole geometries and flow conditions (FIG. 5).)

[0063] The actual underlying mechanism of the membrane is of course significantly more complex due to the neglected coupling between the membrane and the fluid, the effects of fluid loading/damping and the coupling between the fluid above and beneath the membrane. However, the discontinuity at the membrane still holds even when the coupling effect is considered.

## EXPERIMENTAL RESULTS

### Streaming field generated by the acoustic membrane

[0064] FIG. 5 shows the strong acoustic streaming field generated by the membrane with the through hole (the hole is presented by the bright blue circle in FIG. 5(a) and (c)). The corresponding vortices induce rapid mixing of the two different fluids as they flow past the membrane (see Video 1 in ESI for flow visualisation in FIG. 5(a)). Both the orientation of the vortices with respect to the flow and the strength of the vortices have a considerable effect in the mixing performance. Considering the former, the mixing homogeneity is best when the vortices are symmetrical about the direction of the flow (FIG. 5(f)). In contrast, when the vortices are symmetrical about the line perpendicular to the flow direction as in the case of the rectangular hole (FIG. 5(e)), mixing performance significantly decreases.

[0065] In cases with poor mixing, such as in FIG. 5(c), only a fraction of the entering flow passes through the centre of the vortices pair (which is located at the circular hole). The flow portion next to the channel walls is unaffected by the streaming field, resulting in heterogeneous mixing. Nevertheless, the vortices are evidently strongly influenced by the presence of the hole: they are always centred around it, regardless of the hole geometry (FIG. 5(e) and (f)), or whether the hole is offset from the membrane's centre or not (FIG. 5(g)), or even when the flow is going through the hole (FIG. 5(h) and (i)).

[0066] As seen from FIG. 5(a), the chosen transition length for Eq. (3) is a conservative estimate of the transition from unmixed to mixed state. The true measurement would be at the location of the hole, which is rather difficult to obtain. In this analysis, such calculation of $L_{mix}$ is chosen for consistency with previous studies[29,30,32].

**Acoustic membranes with circular holes**

[0067] The mixing performance of the membranes with circular through holes can be characterised. It can be seen from FIG. 6(a) and (b) that, for a given *a/d* ratio, both mixing efficiency and mixing time increase with decreasing *Pe* in most cases. The higher performing membranes, then, would have higher *MI* and lower $t_{mix}$. Most notably, the best circular membrane can achieve a mixing efficiency of 90% and time of 3 ms at 60 μl/min flow rate ($Pe \approx 8333 \pm 3.5\%$), despite an extremely small portion of unmixed fluid remaining at the bottom wall in FIG. 6(ii) (see Video 2 in ESI). The critical role of hole is pronounced: even for the case of the smallest membrane width $a$ = 210 μm and $a/d$ = 3.5 located in a 1000-μm-wide channel, a mixing index of 0.91 is observed, i.e. a 5-fold increase from a continuous, holeless membrane.

**Acoustic membranes with holes of other geometries**

[0068] Since the strength of the vortices and their symmetry around the bulk flow direction (both critical for efficient mixing as outlined above) are strongly dependent on the properties of the through hole, it is logical to expect that mixing is dependent on the hole geometry. FIG. 7 analyses mixing for acoustic membranes with individual square-shaped and rectangular holes, as well as with a pair of square and circular holes. It can be seen that a square hole can generate vortices whose centre line is aligned at 45° to the flow direction, resulting in higher mixing efficiency compared to a rectangular hole. Most notable is the membrane with a pair of square holes: mixing is achieved with $MI$ = 0.86 and $t_{mix}$ = 4ms at 60 μl/min ($Pe \approx 8333 \pm 3/5\%$). While these values are lower than the best obtained with a circular hole membrane, the mixed fluid spans the entire channel width (FIG. 7(ii) compared to FIG. 6(ii)).

**Composite acoustic membranes**

[0069] The geometric properties of the through holes were further modified to enable high throughput operation, which is crucial for example, for industrial applications.

[0070] Furthermore, multiple identical membranes were combined (FIG. 9(a) and FIG. 9(b)) to form a composite membrane and made to vibrate at MHz frequencies to effectively mix different solutions at a total flow-rate of 5 ml/min (FIG.10).

[0071] Another multiple-layer composite device was constructed by stacking two composite membranes on top of each other (as illustrated in FIG. 9(c)). This new construction significantly increases the total flow rate to 10 ml/min (2-fold increase in throughput) and further enhances the mixing efficiency. FIG. 10(c) and FIG. 10(d) demonstrate complete mixing of two liquids at 1.07 MHz actuation.

[0072] The membranes of the composite devices were fabricated using 550-micrometer-thick silicon wafers via a deep reactive ion etching (DRIE) process (FIG. 11). The DRIE process is typically used to create a deep anisotropic etch profile, with near vertical sidewalls. However, when the etched pattern has sharp corners, the anisotropy is lost after a long period of etching. This leads to a semi isotropic profile and enables generation of variable thickness membranes, required for the high throughput operation. This fabrication process ensures that the effective thickness of the membranes is considerably large, resulting in robust devices operating in significantly higher frequencies, affecting the throughput.

**Acoustic membranes with air bubbles at the holes**

[0073] The hole can be covered with an air/liquid interface to trap a bubble (a mechanism similar to the Lateral Cavity Acoustic Transducer[50]), in order to see whether the membrane will behave similarly to a bubble mixer. This can be achieved by intentionally blocking the bottom outlet (originally intended to immerse the membrane in water) from the start. Interestingly, the resultant vortices are completely different from that of both the immersed acoustic membrane and the acoustic bubble.

[0074] Fig. 8 compares the streaming field, mixing performance and flow visualisation of a fully immersed membrane with those of a membrane covered with a bubble (henceforth referred to as the “bubble membrane”). In both cases, each hole generates two vortices,

and the downstream pair is always stronger than the upstream one. The intensity graph shows that the exit flow is clearly divided into two regions of different mixing efficiency. Flow visualisation in FIG. 8(c) also confirms this division, albeit at a different frequency due to a clump of particles stuck at the upstream (right) hole. Note that the total flow rate of the immersed membrane is twice as high as the bubble one's.

[0075] On the other hand, the marked difference in the streaming field between the two cases can be observed even without flow visualisation. With the immersed membrane, the two holes are coupled, the incoming fluid passes over the upstream hole for the former. On the contrary, for the bubble membrane, the upstream hole's streaming field acts as a blockage. Mixing performance of the bubble membrane is also worse: its mixing index is lower than the immersed membrane that is being used at higher flow rates (0.78 at 5 $\mu$l/min compared to 0.81 at 10 $\mu$l/min). This again emphasises the importance of the through hole of the membrane in mixing.

**Table 1** Dimensions of the membranes with circular holes

| *a/d* | *a* ($\mu$m) | *d* ($\mu$m) |
|---|---|---|
| 2.300 | 230 | 100 |
| 3.667 | 440 | 120 |
| 4.250 | 425 | 100 |
| 5.250 | 420 | 80 |
| 2.275 | 455 | 200 |
| 3.500 | 210 | 60 |
| ∞ | 445 | 0 |

## DISCUSSION

[0076] Microstreaming has previously been utilised to induce mixing, such as the bubble mixer[13] or the oscillating sharp-edges[32]. However, the nature of the streaming vortices generated by the acoustic membrane with a through hole is arguably more complicated. It is well-known that streaming can be driven by an oscillating solid structure in a quiescent

fluid, or equivalently a fixed structure in an oscillating fluid.[42] With regards to its application in mixing, Huang *et al.*[32] has shown that the streaming strength increases with decreasing equivalent spring stiffness. Applying this to the system of the present invention, a membrane with the lowest stiffness (found to be the holeless membrane using ANSYS, which agrees with the equivalent stiffness result of a circular membrane with a circular hole[51]) for a given size *a* and thickness *t* should generate the strongest vortices. Yet, the resultant streaming field of this membrane is almost non-existent. Clearly, the vibration of the membrane alone is not a sufficient explanation for the observed mixing behaviour.

[0077] The aforementioned experimental results have shown through simulations and experiments that the hole creates a discontinuity in the boundary conditions on the membrane, leading to a high velocity gradient. This in turn results in a strong body force field that drives the vortical streaming field responsible for mixing.

[0078] While the numerical simulation neglects the fluid-structure coupling, it still gives a reasonably accurate description of the phenomenon. Firstly, the body force field concentrates around the hole's edge (FIG. 4(e)), which arguably justifies why the streaming field is still observed for an offset hole. Secondly, the body force is a result of the first-order velocity gradient. Hence, when the fluid flows through the hole instead of above it, only the unperturbed velocity field $\mathbf{v}_0$ changes, leaving $\mathbf{v}_0$ and thus **F** unchanged. (Only the streaming field pattern $\mathbf{v}_s$ is expected to change.) And thirdly, the "bubble membrane" is likely to have a different deflection mode ($w(x)$ used in Eq. (10c)), and there is no longer coupling of fluid on both sides of the membrane. Consequently, a different streaming behaviour is observed compared to that of an immersed membrane. As to why the vortices appear different from that of a bubble mixer, it can be seen that the edges of the bubbles in the bubble membrane are not fixed, instead they are vibrating together with the edges of the membrane's holes. This leads to a different set of boundary conditions for the bubble, and as a result produces a dissimilar behaviour.

## APPLICATIONS

[0079] Micro-fluidic mixing using the membrane of the present invention can be used to

generate highly uniform and ultrafine nanoparticles offering significant improvements to well-established liquid antisolvent techniques.

[0080] Poor aqueous solubility limits the bioavailability of a significant portion of drug compounds. Reducing the size of drugs to nanometre scales and hence increasing the surface area-to-volume ratio improves the dissolution rate, addressing this significant bottleneck in pharmaceutical industries. Another significant advantage of using nanoparticles is in targeted delivery of drugs to treat lung disease, where it has been shown that size of particles would determine where most of the deposition would take place inside the lung either via oral or nasal inhalation. Many sites of the lung which are hard to treat via conventional drugs can only be reached via particles with customized dimensions.

[0081] A common prior art approach for nanodrug synthesis is the Liquid Anti-Solvent (LAS) method. The method consists of mixing an organic solvent (in which the drug is soluble) with an aqueous fluid to reach supersaturation. The hydrophilic drug precipitates as the anti-solvent is introduced in the system at a fast pace and supersaturation concentration. By contrast, the 3D microfluidic geometry associated with membranes of the present invention can separate the solvent and antisolvent phases. The vibrating membrane results in efficient mixing of the liquid solutions offering significant improvements to conventional LAS methods.

[0082] The performance of the device was demonstrated through a series of experiments to crystallise 140 nm diameter particles of Budesonide (a common asthma drug), with a polydispersity Index smaller than 0.1. This offers a 10-fold reduction in size compared to earlier well established methods of the prior art.

[0083] The device was assembled by sandwiching the chip containing a silicon nitride membrane of the present invention between a PDMS microfluidic channel at the upper side, and an inlet at the underside. The assembled device was then attached to a glass slide (FIG. 12). Budesonide was synthesized, using ethanol as the solvent and MilliQ water as the anti-solvent phase. The membrane was excited by a piezoelectric transducer at its resonant frequency (ranging from 100 – 300 kHz), resulting in strong localized vortices which

effectively mixed the antisolvent and solvent phases while preventing accumulation of the formed particles.

[0084] The particle sizes were characterized through dynamic light scattering (DLS) technology (Malvern Nano-ZS). Budesonide particles with a mean diameter as small as 140 nm were generated reproducibly. This is an approximate 30-fold reduction [52] over well characterized prior art techniques. Very importantly, the polydispersity index (PDI) is below 0.1 demonstrating excellent uniformity without addition of stabilizers. The elimination of surfactant from the process reduces the associated issues of screening for the optimal additives and complicated interaction between the nanoparticles and stabilizers.

[0085] The results show that low concentrations enhance the uniformity of the nanoparticles, however the mean particle diameters are consistently below 200nm for concentrations ranging from 0.2 to 1mg/ml. Similarly, the particle diameter and standard deviation remained consistently low for flow rates ranging between 10 and 50 microliters/min. Parallel operation of multiple mixers can further improve the total flowrate of the mixer while ensure the effectiveness of the acoustic mixer.

[0086] While this invention has been described in connection with specific embodiments thereof, it will be understood that it is capable of further modification(s). This application is intended to cover any variations uses or adaptations of the invention following in general, the principles of the invention and including such departures from the present disclosure as come within known or customary practice within the art to which the invention pertains and as may be applied to the essential features hereinbefore set forth.

[0087] As the present invention may be embodied in several forms without departing from the spirit of the essential characteristics of the invention, it should be understood that the above described embodiments are not to limit the present invention unless otherwise specified, but rather should be construed broadly within the spirit and scope of the invention as defined in the appended claims. The described embodiments are to be considered in all respects as illustrative only and not restrictive.

[0088] Various modifications and equivalent arrangements are intended to be included within the spirit and scope of the invention and appended claims. Therefore, the specific embodiments are to be understood to be illustrative of the many ways in which the principles of the present invention may be practiced. In the following claims, means-plus-function clauses are intended to cover structures as performing the defined function and not only structural equivalents, but also equivalent structures.

[0089] "Comprises/comprising" and "includes/including" when used in this specification is taken to specify the presence of stated features, integers, steps or components but does not preclude the presence or addition of one or more other features, integers, steps, components or groups thereof. Thus, unless the context clearly requires otherwise, throughout the description and the claims, the words 'comprise', 'comprising', 'includes', 'including' and the like are to be construed in an inclusive sense as opposed to an exclusive or exhaustive sense; that is to say, in the sense of "including, but not limited to".

**References**

[1] K. F. Jensen, S. L. Firebaugh, A. J. Franz, D. Quiram, R. Srinivasan and M. A. Schmidt, Micro Total Analysis Systems 98, 1998, pp. 463–468.

[2] L. Pollack, M. W. Tate, N. C. Darnton, J. B. Knight, S. M. Gruner, W. A. Eaton and R. H. Austin, *Proc. Natl. Acad. Sci. U.S.A.*, 1999, **96**, 10115–10117. [3] R. Karnik, F. Gu, P. Basto, C. Cannizzaro, L. Dean, W. Kyei-Manu, R. Langer and O. C. Farokhzad, *Nano Lett.*, 2008, **8**, 2906–2912.

[4] N. M. Belliveau, J. Huft, P. J. Lin, S. Chen, A. K. Leung, T. J. Leaver, A. W. Wild, J. B. Lee, R. J. Taylor, Y. K. Tam *et al.*, *Mol Ther Nucleic Acids*, 2012, **1**, e37.

[5] J.-M. Lim and R. Karnik, *Nanomedicine*, 2014, **9**, 1113–1116.

[6] J. M. Ottino and S. Wiggins, *Philos Trans A Math Phys Eng Sci*, 2004, **362**, 923–935.

[7] J. B. Knight, A. Vishwanath, J. P. Brody and R. H. Austin, *Phys. Rev. Lett.*, 1998, **80**, 3863.

[8] A. D. Stroock, S. K. Dertinger, A. Ajdari, I. Mezic′, H. A. Stone and G. M. Whitesides, *Science*, 2002, **295**, 647–651. [9] H. Wang, P. Iovenitti, E. Harvey and S. Masood, *Smart Mater. Struct.*, 2002, **11**, 662.

[10] C.-P. Jen, C.-Y. Wu, Y.-C. Lin and C.-Y. Wu, *Lab Chip*, 2003, **3**, 77–81.

[11] Y. Z. Liu, B. J. Kim and H. J. Sung, *Int. J. Heat Fluid Flow*, 2004, **25**, 986–995.

[12] B. He, B. J. Burke, X. Zhang, R. Zhang and F. E. Regnier, *Anal. Chem.*, 2001, **73**, 1942–1947.

[13] R. H. Liu, J. Yang, M. Z. Pindera, M. Athavale and P. Grodzinski, *Lab Chip*, 2002, **2**, 151–157.

[14] C.-H. Tai, R.-J. Yang, M.-Z. Huang, C.-W. Liu, C.-H. Tsai and L.-M. Fu, *Electrophoresis*, 2006, **27**, 4982–4990.

[15] Y. Wang, J. Zhe, B. T. Chung and P. Dutta, *Microfluid Nanofluidics*, 2008, **4**, 375–389.

[16] S. Oberti, A. Neild and T. W. Ng, *Lab Chip*, 2009, **9**, 1435–1438.

[17] A. Neild, T. W. Ng, G. J. Sheard, M. Powers and S. Oberti, *Sens. Actuators, B*, 2010, **150**, 811–818.

[18] N.-T. Nguyen and Z. Wu, *J. Micromech. Microeng.*, 2005, **15**, R1.

[19] C.-Y. Lee, C.-L. Chang, Y.-N. Wang and L.-M. Fu, *Int J Mol Sci*, 2011, **12**, 3263–3287.

[20] M. Wiklund, C. Gu¨nther, R. Lemor, M. Ja¨ger, G. Fuhr and H. M. Hertz, *Lab Chip*,

2006, **6**, 1537–1544.

[21] T. Laurell, F. Petersson and A. Nilsson, *Chem. Soc. Rev.*, 2007, **36**, 492–506.

[22] R. Walker, I. Gralinski, K. K. Lay, T. Alan and A. Neild, *Appl. Phys. Lett.*, 2012, **101**, 163504.

[23] P. Rogers and A. Neild, *Lab Chip*, 2011, **11**, 3710–3715.

[24] D. J. Collins, T. Alan and A. Neild, *Lab Chip*, 2014, **14**, 1595–1603.

[25] X. Ding, Z. Peng, S.-C. S. Lin, M. Geri, S. Li, P. Li, Y. Chen, M. Dao, S. Suresh and T. J. Huang, *Proc. Natl. Acad. Sci. U.S.A.*, 2014, **111**, 12992–12997.

[26] H. V. Phan, M. S¸ es¸en, T. Alan and A. Neild, *Appl. Phys. Lett.*, 2014, **105**, 193507.

[27] K. Sritharan, C. Strobl, M. Schneider, A. Wixforth and Z. v. Guttenberg, *Appl. Phys. Lett.*, 2006, **88**, 054102.

[28] S. S. Wang, Z. J. Jiao, X. Y. Huang, C. Yang and N. T. Nguyen, *Microfluid Nanofluidics*, 2009, **6**, 847–852.

[29] D. Ahmed, X. Mao, J. Shi, B. K. Juluri and T. J. Huang, *Lab Chip*, 2009, **9**, 2738–2741.

[30] D. Ahmed, X. Mao, B. K. Juluri and T. J. Huang, *Microfluid Nanofluidics*, 2009, **7**, 727–731.

[31] M. C. Jo and R. Guldiken, *Sens. Actuators, A*, 2013, **196**, 1–7.

[32] P.-H. Huang, Y. Xie, D. Ahmed, J. Rufo, N. Nama, Y. Chen, C. Y. Chan and T. J. Huang, *Lab Chip*, 2013, **13**, 3847–3852.

[33] A. Ozcelik, D. Ahmed, Y.-L. Xie, N. Nama, Z. Qu, A. A. Nawaz and T. J. Huang, *Anal. Chem.*, 2014.

[34] H. Jagannathan, G. G. Yaralioglu, A. S. Ergun, F. Degertekin and B. Khuri-Yakub, Ultrasonics Symposium, 2001 IEEE, 2001, pp. 859–862.

[35] G. G. Yaralioglu, I. O. Wygant, T. C. Marentis and B. T. Khuri-Yakub, *Anal. Chem.*, 2004, **76**, 3694–3698.

[36] J. Creemer, F. Santagata, B. Morana, L. Mele, T. Alan, E. Iervolino, G. Pandraud and P. Sarro, Micro Electro Mechanical Systems (MEMS), 2011 IEEE 24th International Conference on, 2011, pp. 1103–1106.

[37] T. Yokosawa, T. Alan, G. Pandraud, B. Dam and H. Zandbergen, *Ultramicroscopy*, 2012, **112**, 47–52.

[38] T. Alan, T. Yokosawa, J. Gaspar, G. Pandraud, O. Paul, F. Creemer, P. M. Sarro and H. W. Zandbergen, *Appl. Phys. Lett.*, 2012, **100**, 081903.

[39] T.-D. Luong, V.-N. Phan and N.-T. Nguyen, *Microfluidics and nanofluidics*, 2011, **10**, 619–625.

[40] A. Hashmi and J. Xu, *J Lab Autom*, 2014, **19**, 488–491.

[41] N.-T. Nguyen and R. M. White, *Ultrasonics, Ferroelectrics, and Frequency Control, IEEE Transactions on*, 2000, **47**, 1463–1471.

[42] W. Nyborg, *Physical acoustics*, 1965, **2**, 265.

[43] P. Agrawal, P. S. Gandhi and A. Neild, *Physical Review Applied*, 2014, **2**, 064008.

[44] C. Devendran, I. Gralinski and A. Neild, *Microfluid Nanofluidics*, 2014, 1–12.

[45] P. M. Morse and K. U. Ingard, *Theoretical acoustics*, Princeton university press, 1968.

[46] P. B. Muller, R. Barnkob, M. J. H. Jensen and H. Bruus, *Lab Chip*, 2012, **12**, 4617–4627.

[47] A. W. Leissa, *Vibration of plates*, Dtic document technical report, 1969.

[48] R. Moroney, R. White and R. Howe, *Applied physics letters*, 1991, **59**, 774–776.

[49] L. Pan, T. Ng, G. Liu, K. Lam and T. Jiang, *Sensors and Actuators A: Physical*, 2001, **93**, 173–181.

[50] A. R. Tovar and A. P. Lee, *Lab Chip*, 2009, **9**, 41–43.

[51] S. Timoshenko and S. Woinowsky-Krieger, *Theory of plates and shells*

[52] T. T. Hu, H. Zhao, L.C. Jiang, Y. Le, J.F. Chen, J. Yun, *Engineering Pharmaceutical Fine Particles of Budesonide for Dry Powder Inhalation (DPI)*, Industrial and Engineering Chemistry Research, 47, 9623-9627 (2008)

## CLAIMS

1. A membrane for microfluidic mixing, having an upper membrane surface and a lower membrane surface and comprising at least one discontinuity.

2. A membrane according to claim 1 wherein the discontinuity is a hole in boundary conditions of said membrane and located between said upper membrane surface and lower membrane surface.

3. A membrane according to claim 1 or claim 2 comprising micro-fabricated silicon nitride or silicon.

4. A membrane according to claim 1 wherein the discontinuity is defined by a periphery of polygonal shape or closed symmetric curve shape.

5. A membrane according to any one of the preceding claims wherein the membrane generates a vortical acoustic streaming field when subjected to acoustic excitations.

6. A membrane according to claim 5 wherein the membrane exhibits transverse vibrations when subjected to acoustic excitations.

7. A membrane according to claim 6 wherein the vortical acoustic streaming field comprises vortices having a plane perpendicular to the direction of the transverse vibrations of the membrane.

8. A membrane according to any one of the previous claims having two or more discontinuities.

9. An acoustic mixer comprising at least one membrane of any one of the previous claims.

10. A composite membrane for microfluidic mixing comprising two or more membranes according to any one of claims 1 to 8.

11 A microfluidic chip comprising at least one membrane of any one of claims 1 to 8 and a piezoelectric disk for applying acoustic excitation to the membrane.

12 A method of mixing comprising the steps of:

(i) immersing the membrane of any one of claims 1 to 8 in a fluid,

(ii) applying acoustic excitation to the fluid such that the membrane exhibits transverse vibrations and a streaming field in the form of vortices is generated.

13. A method according to claim 12, wherein efficiency of the mixing is >80%, preferably >90% in 3 ms at a fluid flow rate of 60 $\mu$l/min.

14. A method according to claim129, wherein efficiency of the mixing is >80%, preferably >86% in 4 ms at a fluid flow rate of 60 $\mu$l/min.

15. A method according to claim 12 when used for rapid mixing of fluids or nano-dispersal.

16. A method of manufacturing the membrane of any one of claims 1 to 8, the method comprising the steps of:

(i) coating an upper surface of a silicon wafer with a photoresistant substance,

(ii) carrying our photolithography to expose a predetermined peripheral shape of a discontinuity on the upper surface,

(iii) etching the exposed shape to create the discontinuity in the form of a hole defined by the discontinuity and extending from the upper surface to a lower

surface of the silicon wafer, and

(iv) removing the photoresistant substance from the silicon wafer.

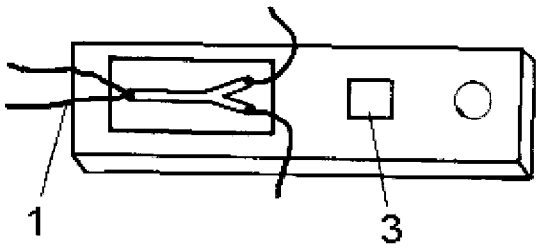



FIG. 1a

FIG. 1c

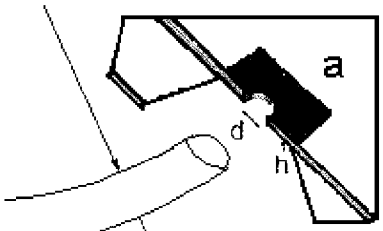
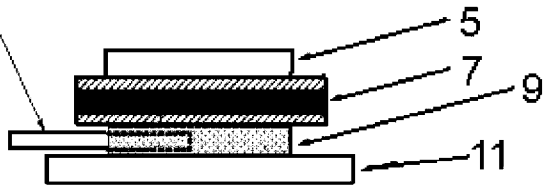



FIG. 1d



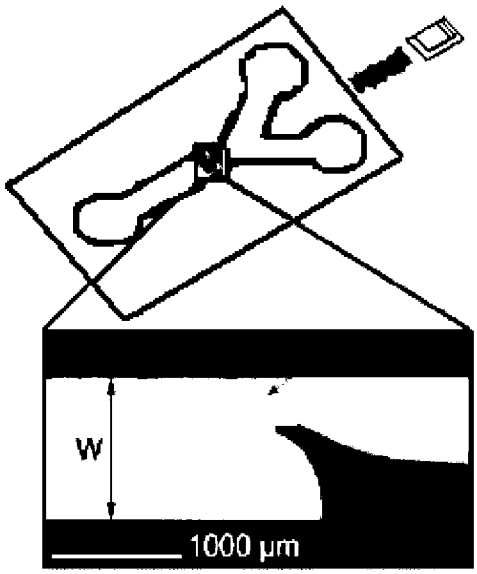




FIG. 1b

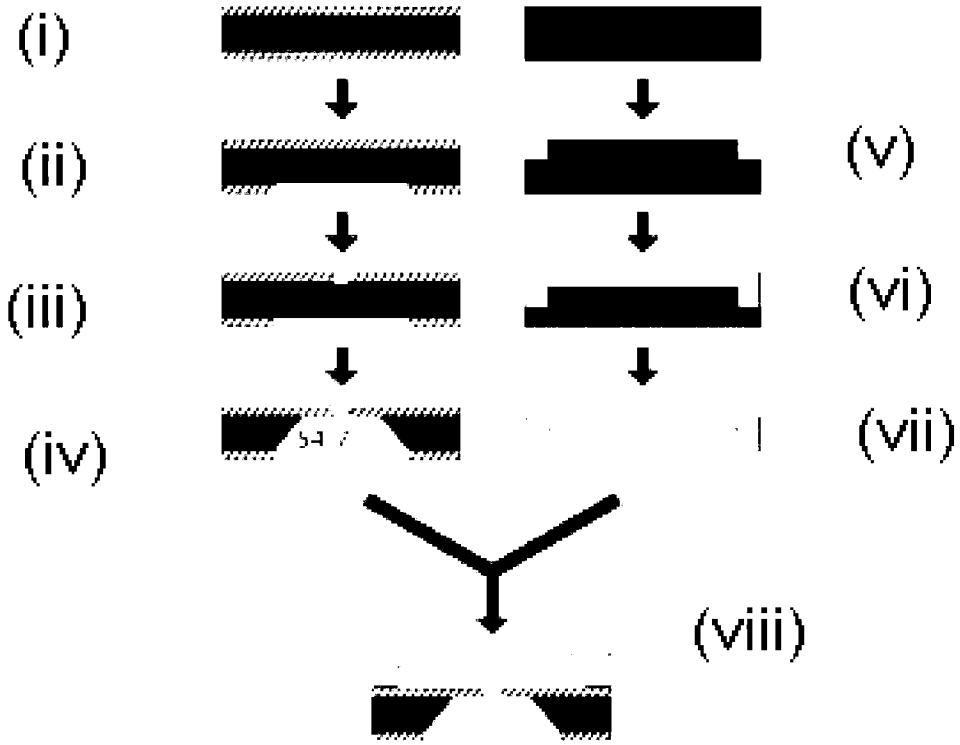



FIG. 1e

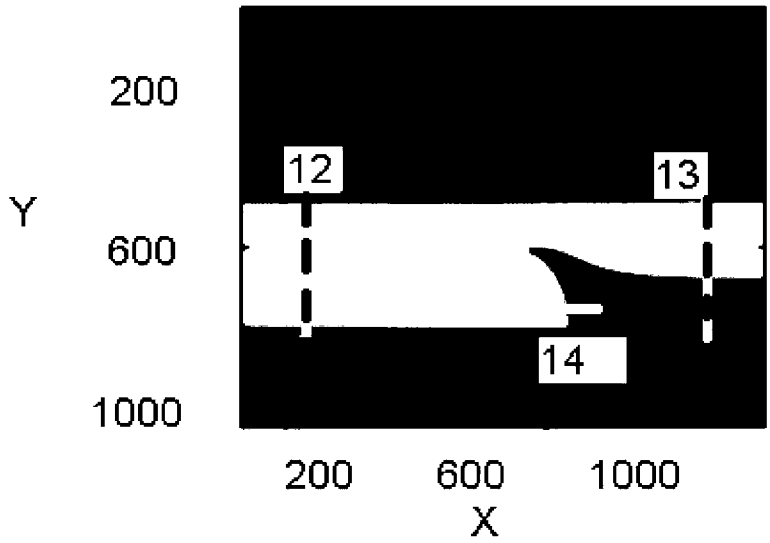



FIG. 2a

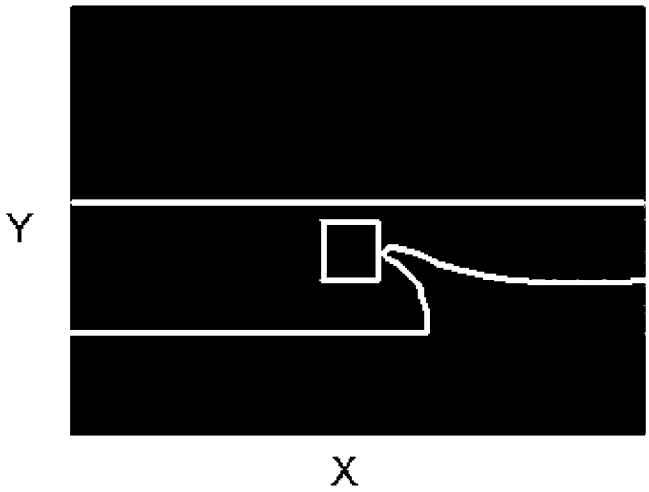



FIG. 2b

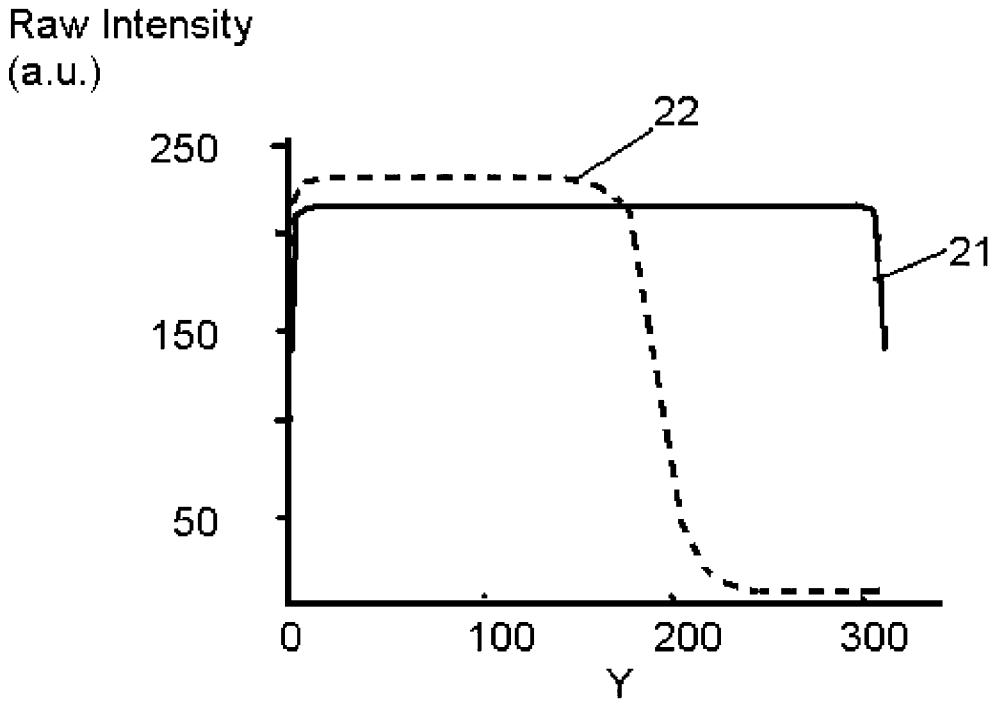

Raw Intensity
(a.u.)
250
150
50
0
100
200
300
Y
22
21

FIG. 2c

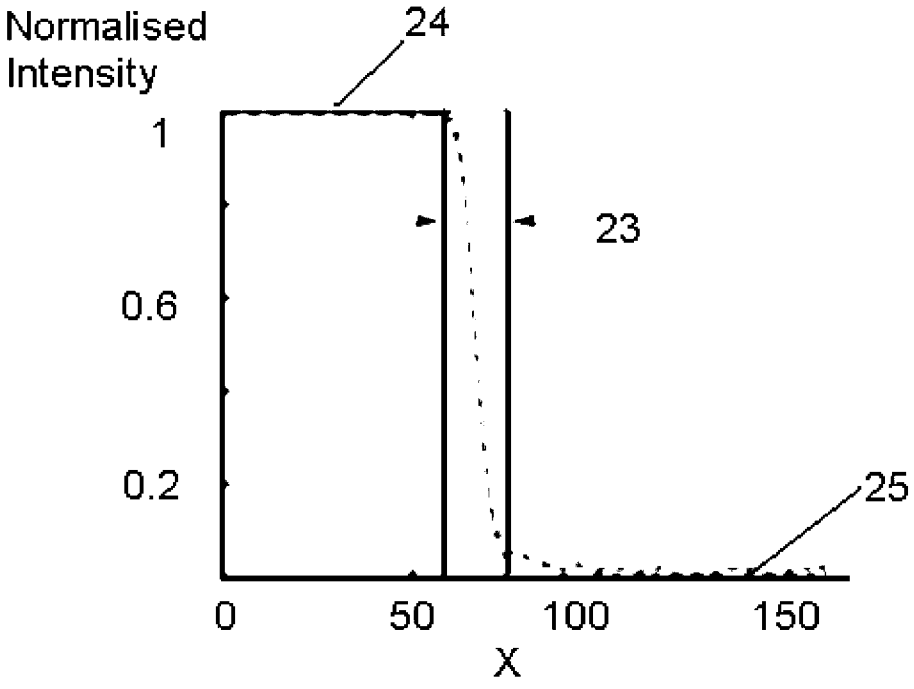

Normalised
Intensity
1
0.6
0.2
0
50
100
150
X
24
23
25

FIG. 2d

FIG. 3a

FIG. 3b

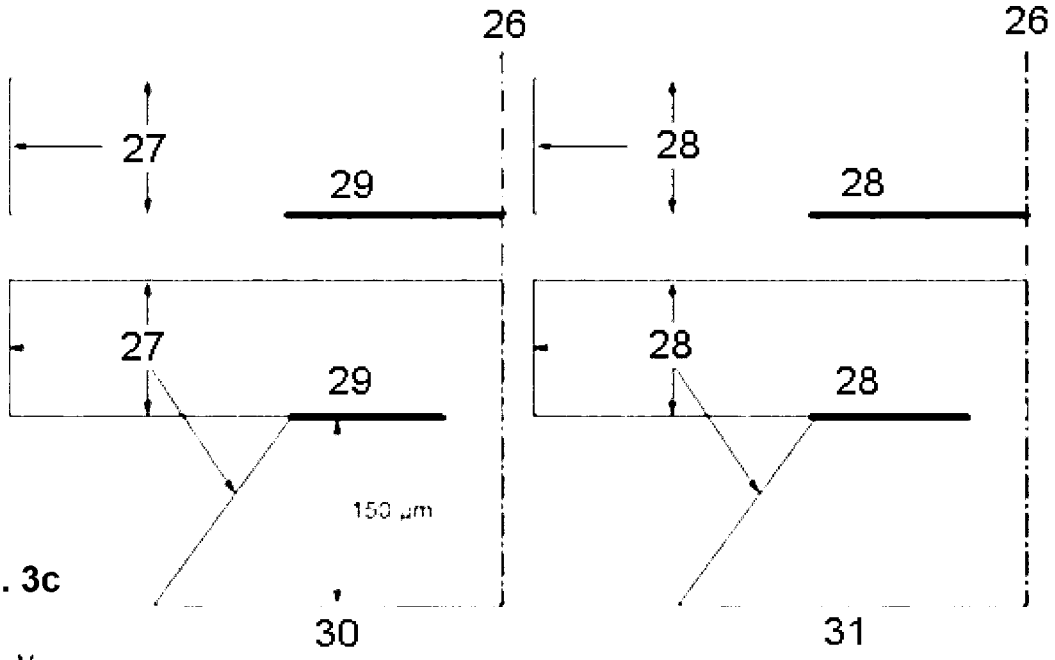
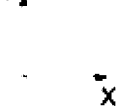



FIG. 3c



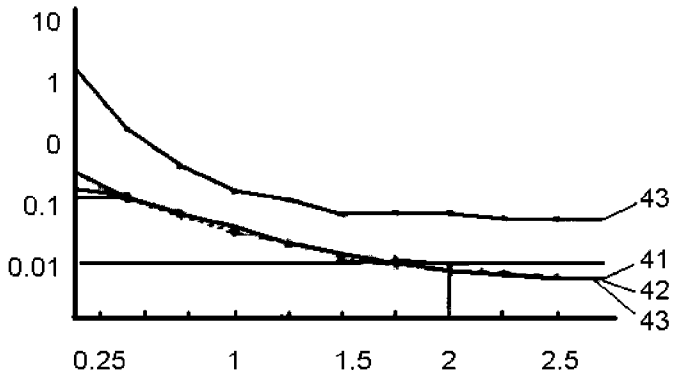



FIG. 4a

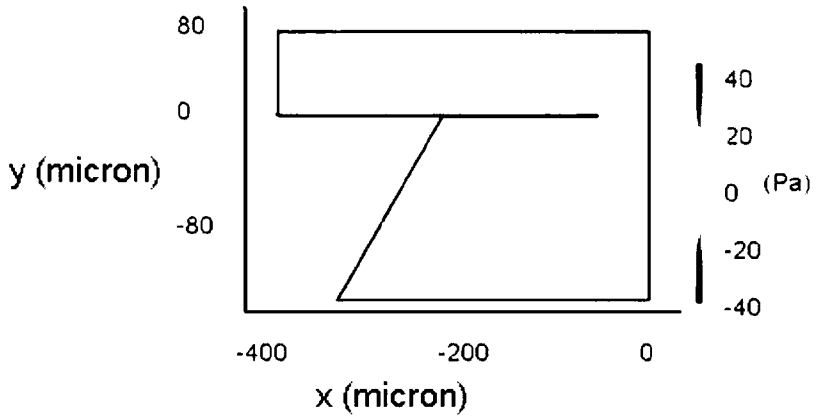



FIG. 4b

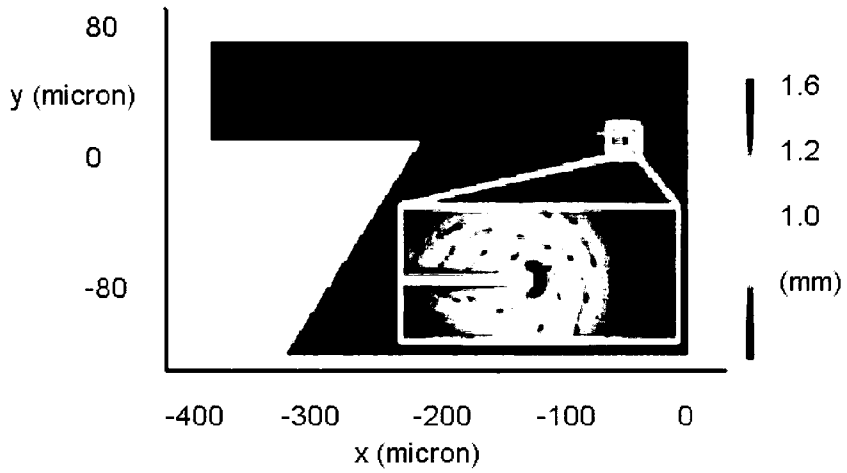



FIG. 4c

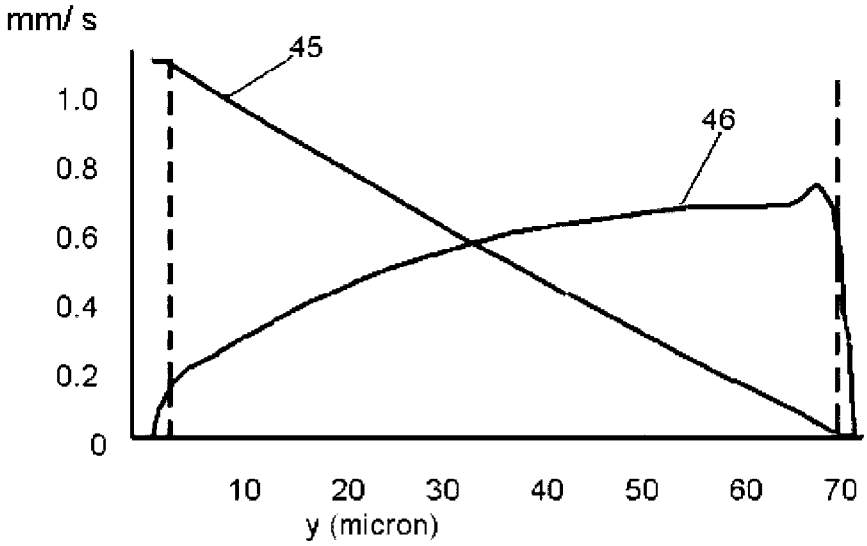

mm/ s
45
46
1.0
0.8
0.6
0.4
0.2
0
10
20
30
40
50
60
70
y (micron)

FIG. 4d

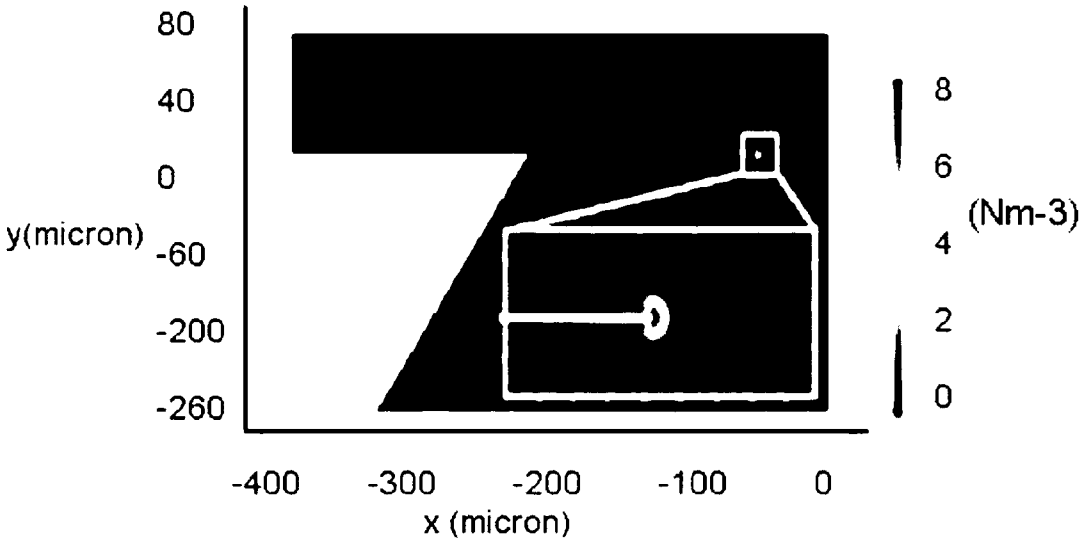

80
40
0
y(micron)
-60
-200
-260
-400
-300
-200
-100
0
x (micron)
8
6
4
2
0
(Nm-3)

FIG. 4e

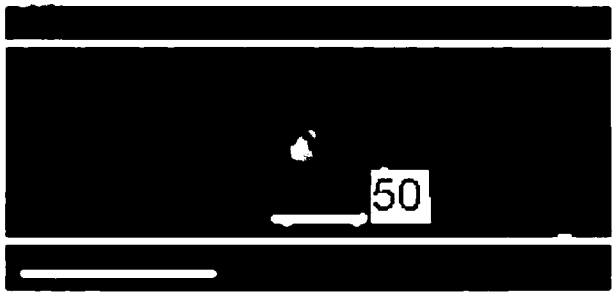



FIG. 5a



FIG. 5b

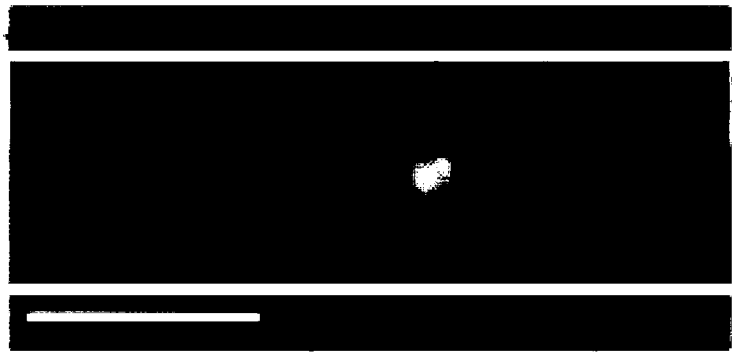


FIG. 5c

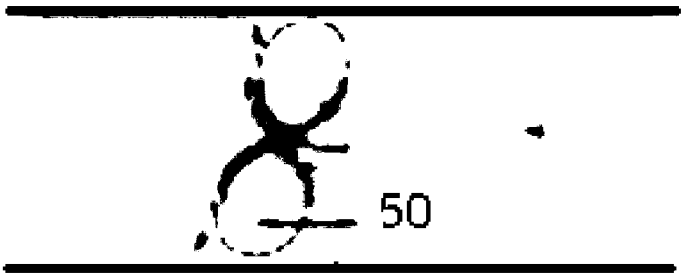



FIG. 5d

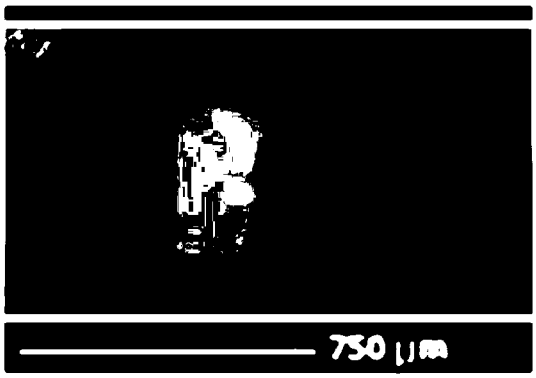



FIG. 5e

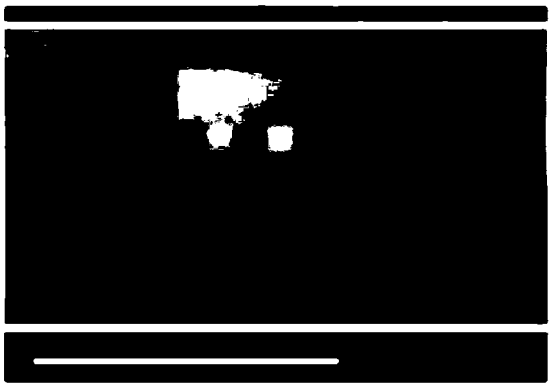


FIG. 5f



FIG. 5g




FIG. 5h




FIG. 5i

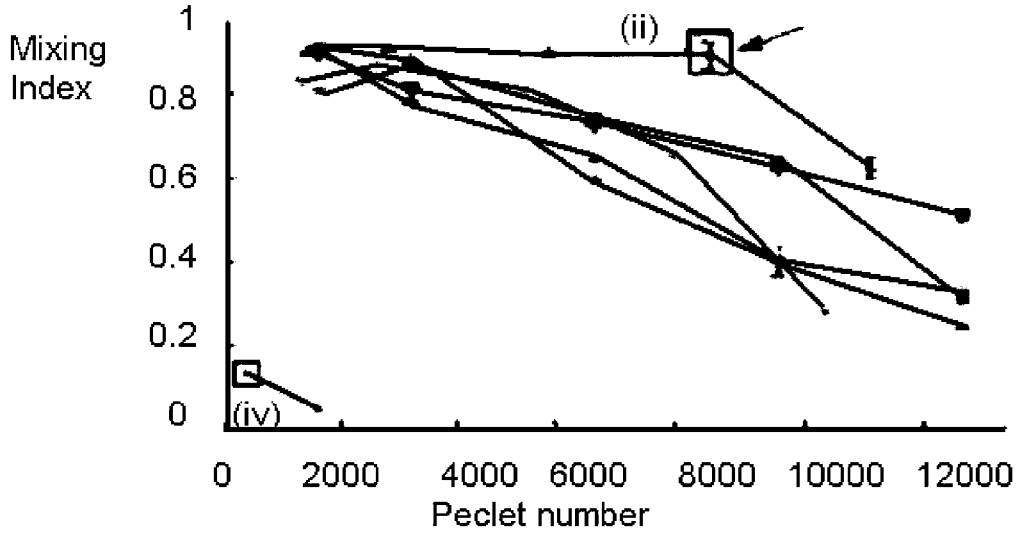

Mixing Index
1
0.8
0.6
0.4
0.2
0
(ii)
(iv)
0
2000
4000
6000
8000
10000
12000
Peclet number

FIG. 6a


1000 μm
1000 μm

(i) (ii)

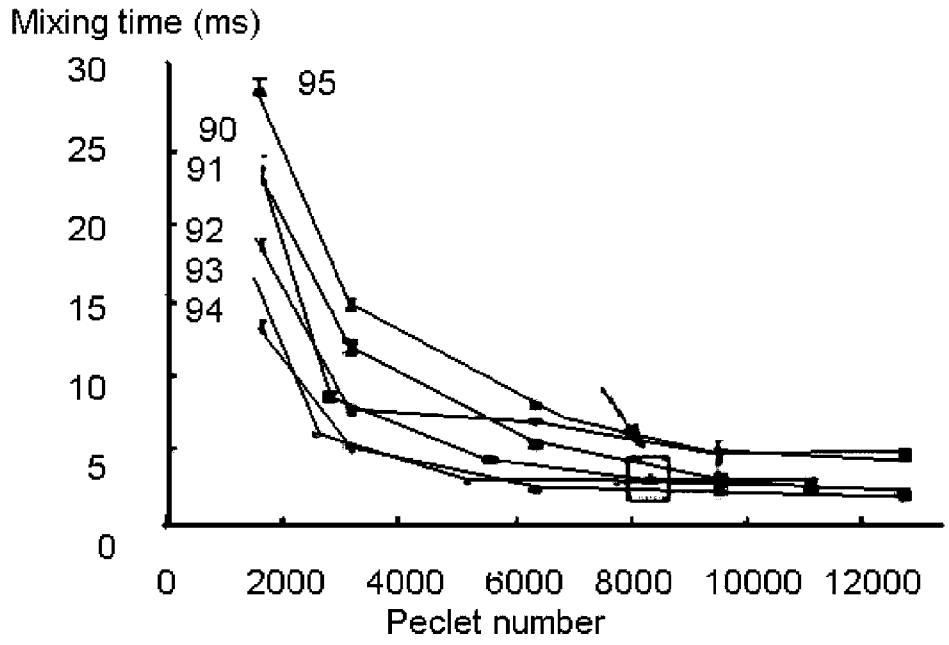

Mixing time (ms)
30
25
20
15
10
5
0
95
90
91
92
93
94
0
2000
4000
6000
8000
10000
12000
Peclet number

FIG. 6b


750 µm
750 µm

(iii) (iv)

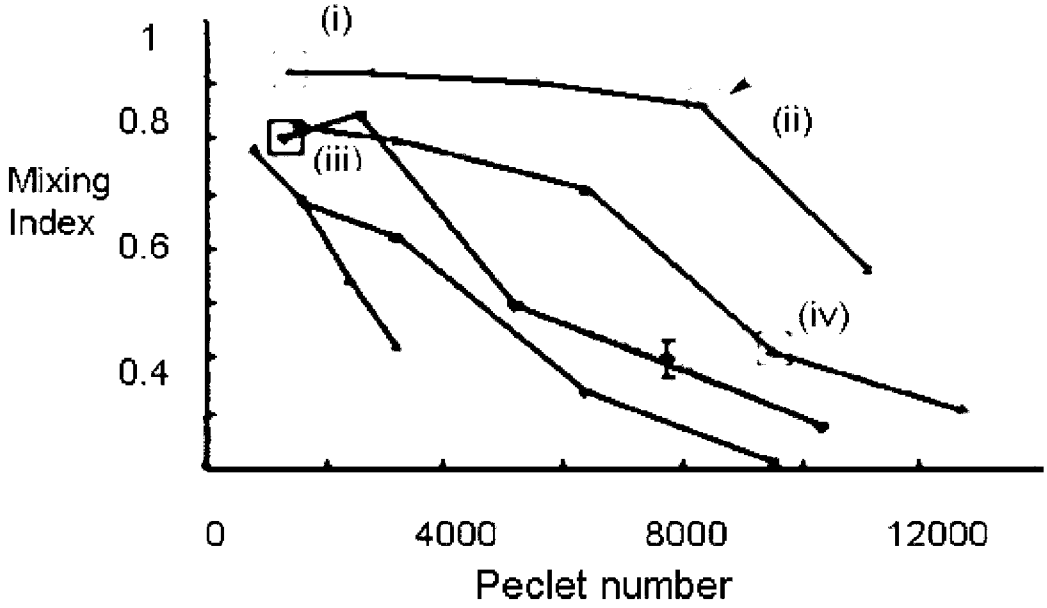
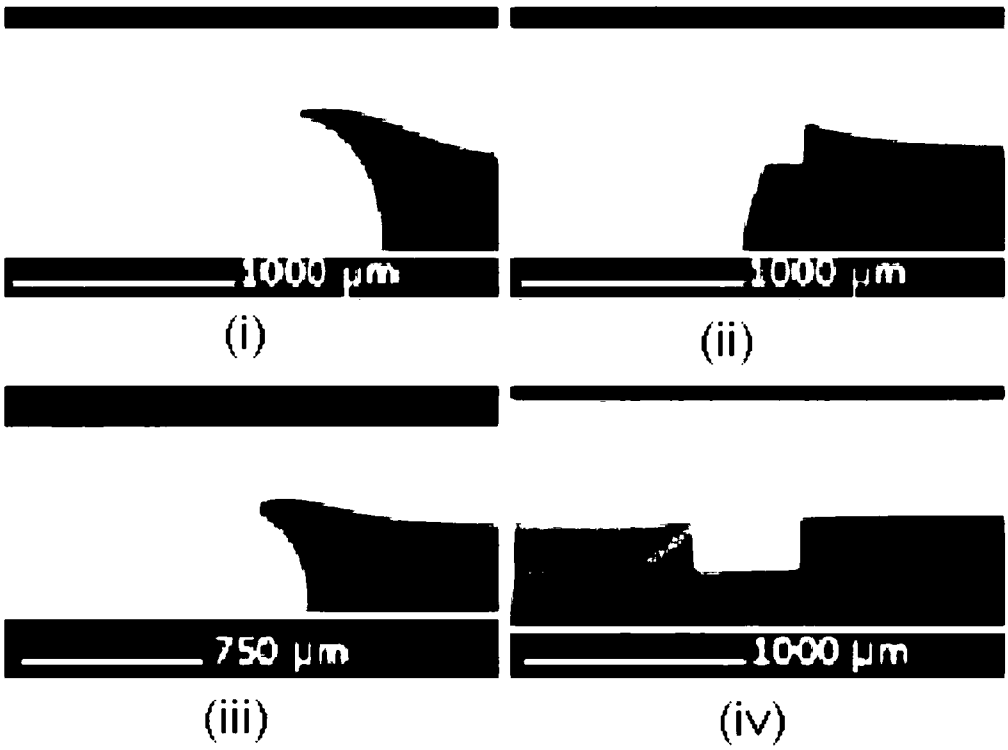

(i)
(ii)
(iii)
(iv)
1
0.8
0.6
0.4
Mixing Index
0
4000
8000
12000
Peclet number

FIG. 7a


1000 µm
(i)
1000 µm
(ii)
750 µm
(iii)
1000 µm
(iv)

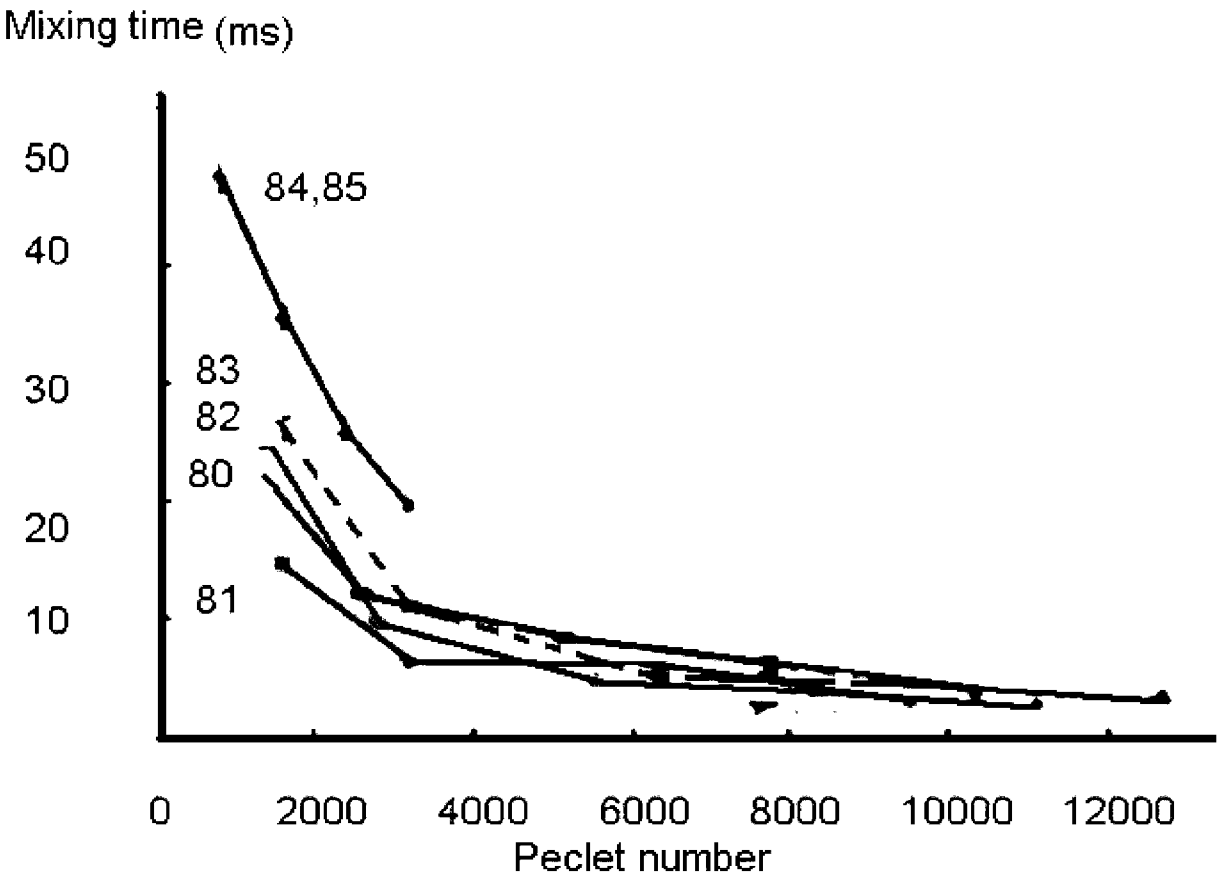
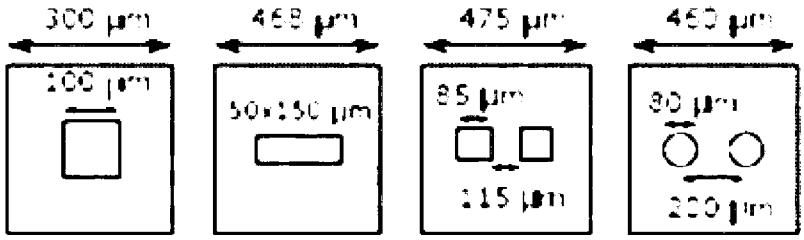



FIG. 7b




(80) (81) (82) (83)

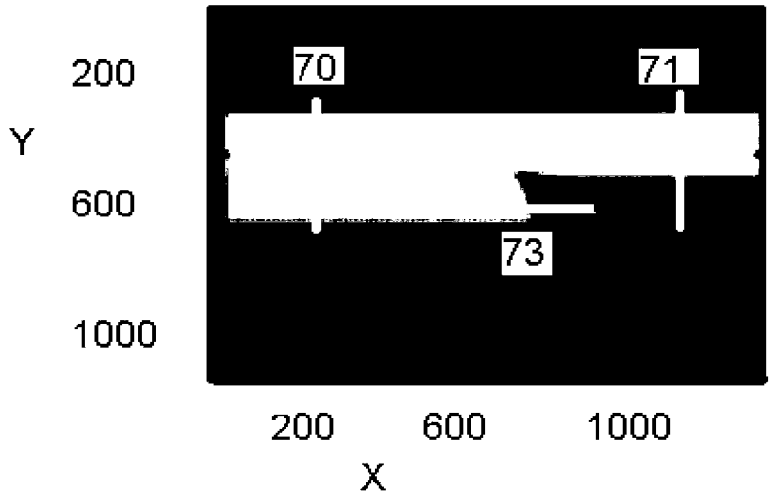

70
71
73
200
Y
600
1000
200
600
1000
X

FIG. 8a

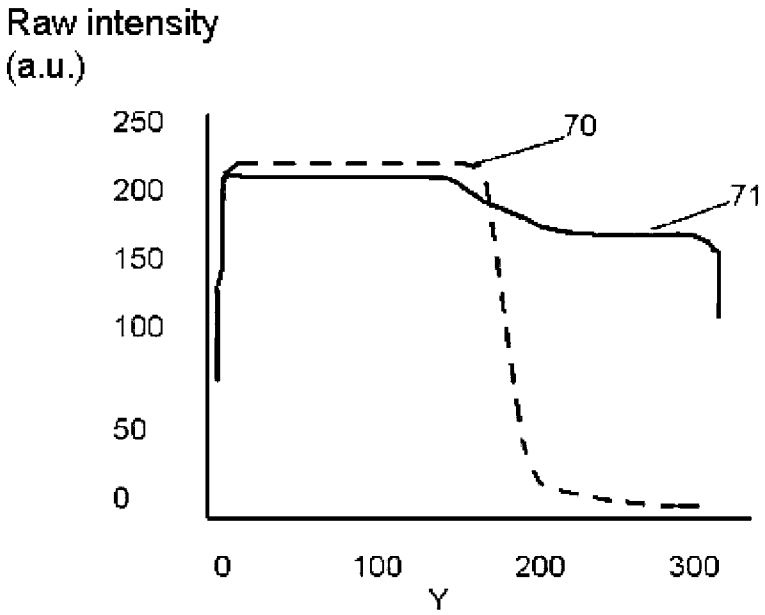

Raw intensity
(a.u.)
250
200
150
100
50
0
70
71
0
100
200
300
Y

FIG. 8b

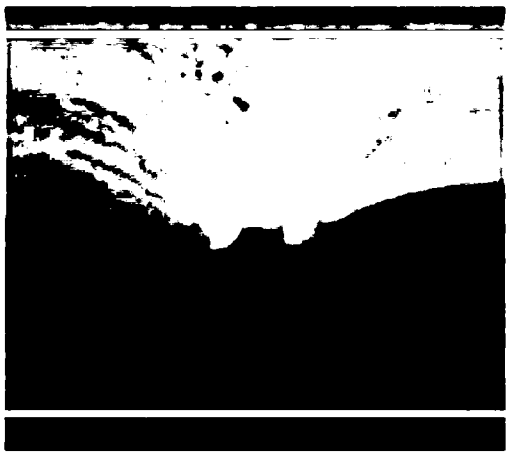


FIG. 8c

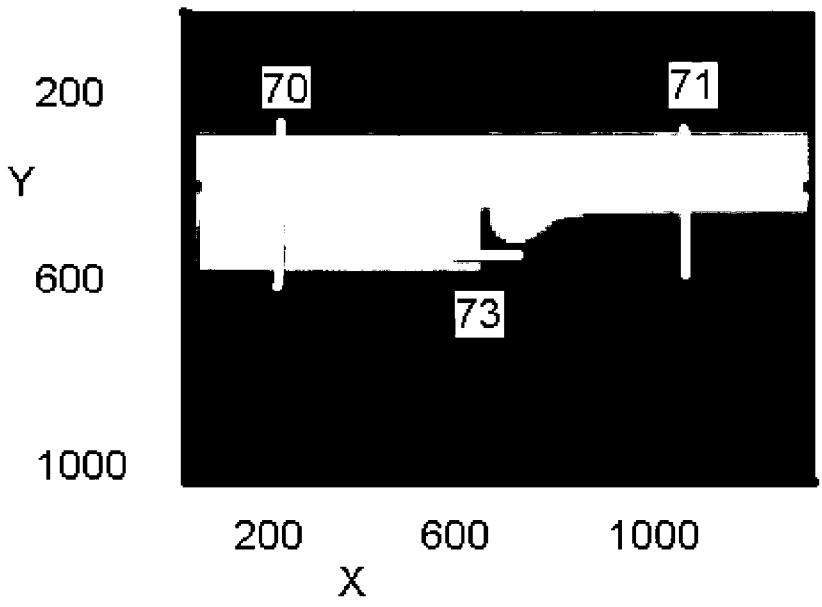



FIG. 8d

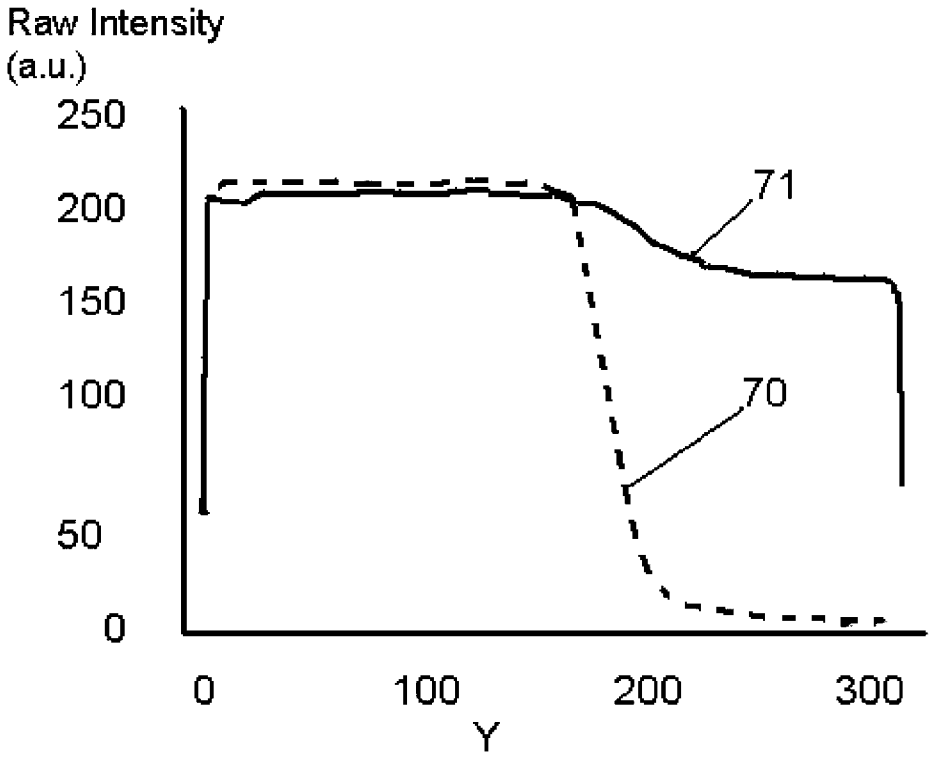



FIG. 8e



FIG. 8f

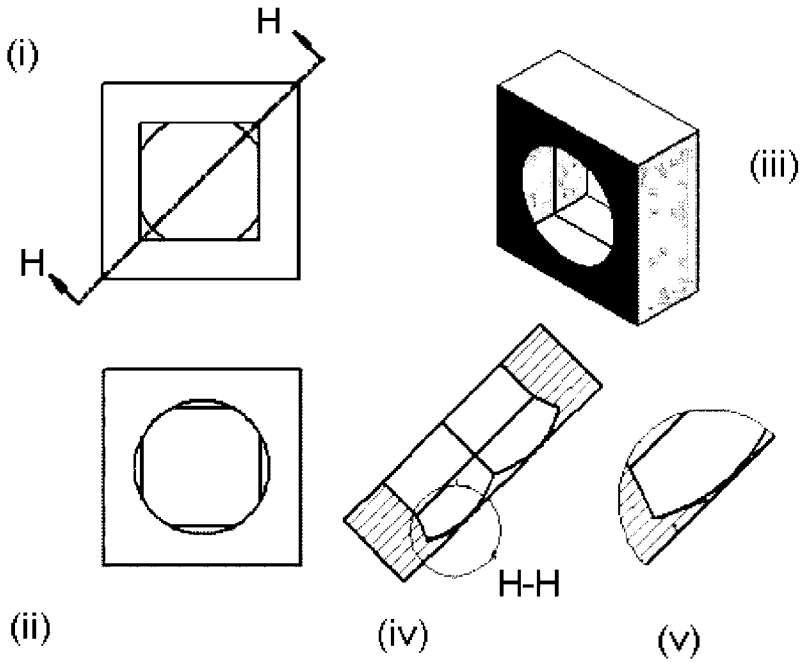



FIG. 9a

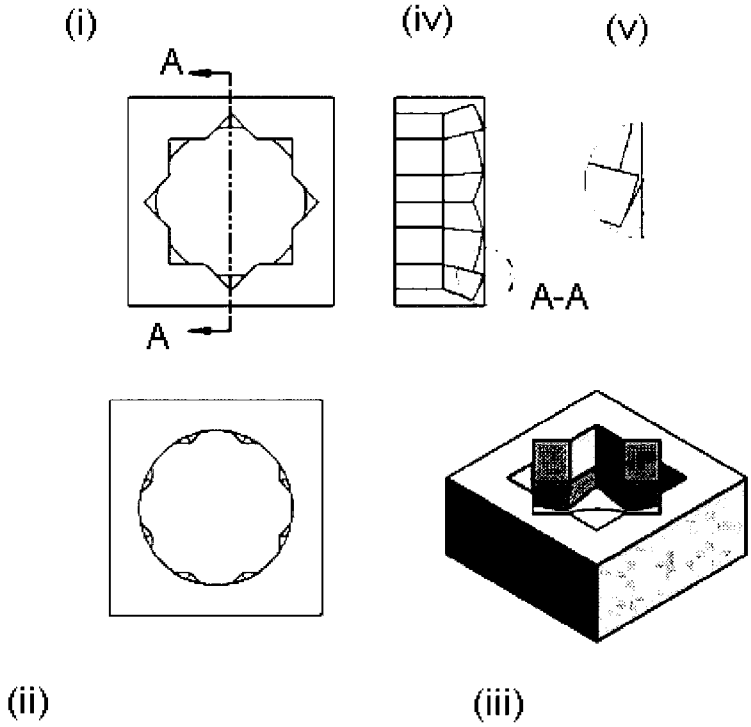
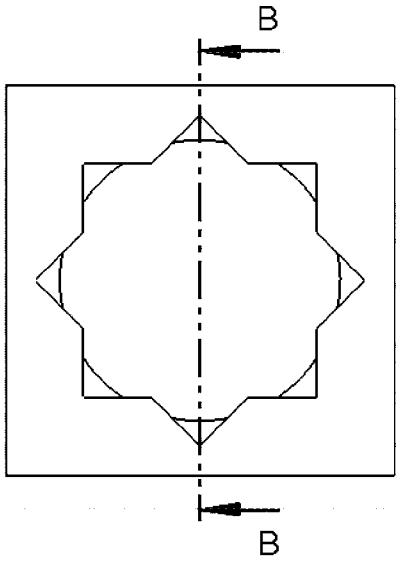
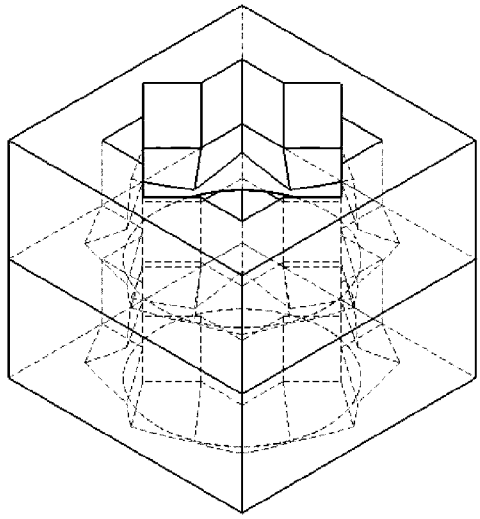



FIG. 9b

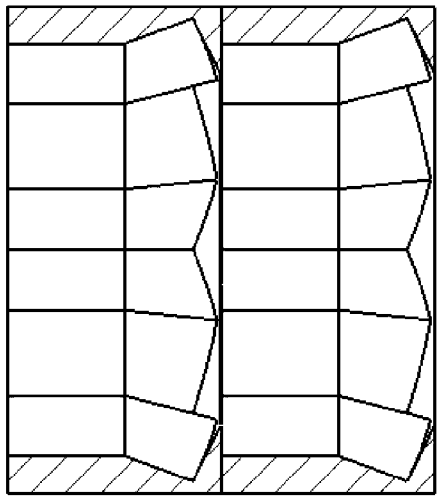
FIG. 9c




(i)



(ii)



(iii)

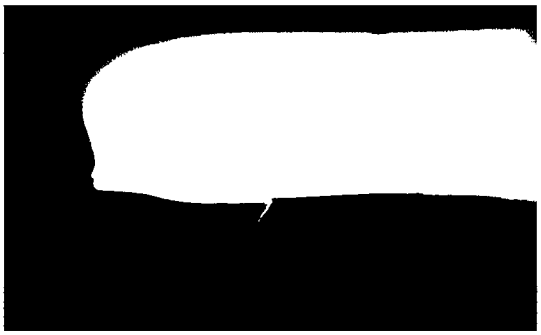


FIG. 10a



FIG. 10b



FIG. 10c

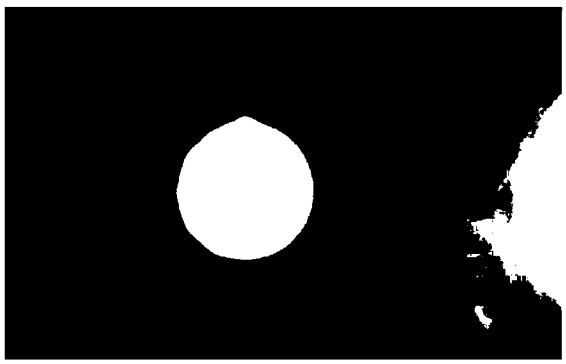


FIG. 10d

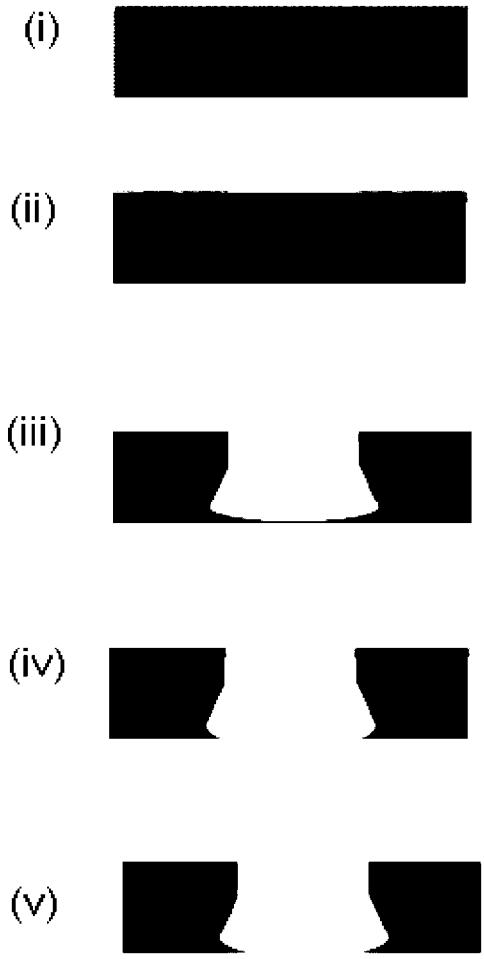



FIG. 11

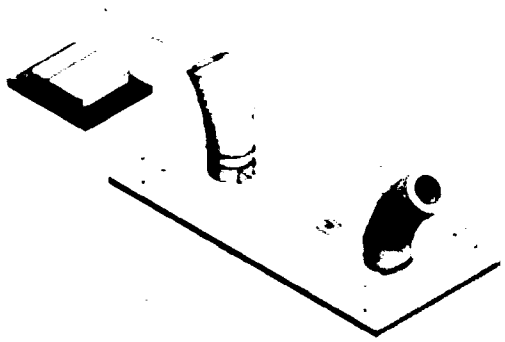


FIG. 12a

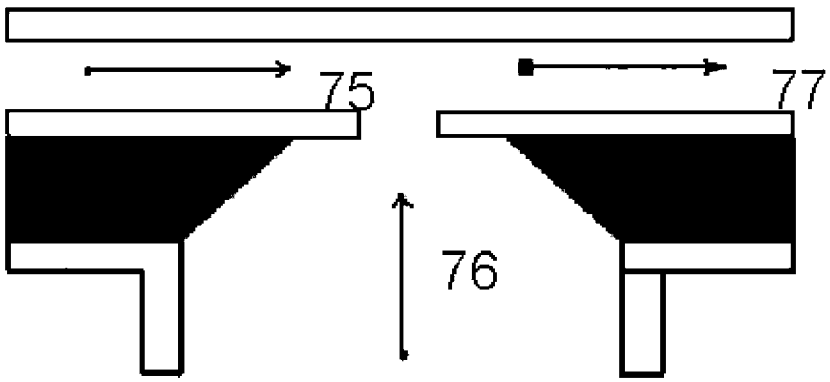



FIG. 12b

**INTERNATIONAL SEARCH REPORT**

International application No.
**PCT/AU2016/000299**

A. CLASSIFICATION OF SUBJECT MATTER

***B01F 11/02 (2006.01)  B01F 13/00 (2006.01)  B01J 19/10 (2006.01)***

According to International Patent Classification (IPC) or to both national classification and IPC

B. FIELDS SEARCHED

Minimum documentation searched (classification system followed by classification symbols)

Documentation searched other than minimum documentation to the extent that such documents are included in the fields searched

Electronic data base consulted during the international search (name of data base and, where practicable, search terms used)

Database : WPIAP and EPODOC; IPC and CPC: B01F13/0059, B01F11/0258, Y10S366/04, B01F11/02, BO1F13/00, B01J19/10, B01F11/0045, B01F11/0266, B01F11/0034, B01F11/0062, B01F15/00493 using keywords such as: microfluidic, mixing, membrane, acoustic and their similar keywords. AusPat, Google Patents, Espacenet, ScienceDirect, YouTube, and Google Scholar were searched using keywords such as: microfluidic, micro mixing, hole, acoustic, vortex, chip, silicon, lithography, efficiency and their similar keywords. AusPat, USPTO, Espacenet and in internal databases provided by IP Australia were searched for applicant/inventor: Monash University, Hoang Van Phan, Bulut Coskun, Adrian Neild, Tuncay Alan, and Hoai An Le Nguyen.

C. DOCUMENTS CONSIDERED TO BE RELEVANT

| Category* | Citation of document, with indication, where appropriate, of the relevant passages | Relevant to claim No. |
|---|---|---|
| | Documents are listed in the continuation of Box C | |

[X] Further documents are listed in the continuation of Box C  [X] See patent family annex

* Special categories of cited documents:

"A" document defining the general state of the art which is not considered to be of particular relevance

"E" earlier application or patent but published on or after the international filing date

"L" document which may throw doubts on priority claim(s) or which is cited to establish the publication date of another citation or other special reason (as specified)

"O" document referring to an oral disclosure, use, exhibition or other means

"P" document published prior to the international filing date but later than the priority date claimed

"T" later document published after the international filing date or priority date and not in conflict with the application but cited to understand the principle or theory underlying the invention

"X" document of particular relevance; the claimed invention cannot be considered novel or cannot be considered to involve an inventive step when the document is taken alone

"Y" document of particular relevance; the claimed invention cannot be considered to involve an inventive step when the document is combined with one or more other such documents, such combination being obvious to a person skilled in the art

"&" document member of the same patent family

| Date of the actual completion of the international search | Date of mailing of the international search report |
|---|---|
| 30 November 2016 | 30 November 2016 |
| **Name and mailing address of the ISA/AU** | **Authorised officer** |
| AUSTRALIAN PATENT OFFICE<br>PO BOX 200, WODEN ACT 2606, AUSTRALIA<br>Email address: pct@ipaustralia.gov.au | Abdulla Al-Motin<br>AUSTRALIAN PATENT OFFICE<br>(ISO 9001 Quality Certified Service)<br>Telephone No. 0262837965 |

| INTERNATIONAL SEARCH REPORT<br>C (Continuation). DOCUMENTS CONSIDERED TO BE RELEVANT | | International application No.<br>**PCT/AU2016/000299** |
|---|---|---|
| Category* | Citation of document, with indication, where appropriate, of the relevant passages | Relevant to claim No. |
| X | WO 2009/122340 A1 (KONINKLIJKE PHILIPS ELECTRONICS N.V.) 08 October 2009<br>(Abstract; page 4, lines 17-31; page 7, lines 18-31; page 8, lines 19-31; figures 1-6 and claims 1-14) | 1-16 |
| X | US 8240907 B2 (GABL R. et al.) 14 August 2012<br>(Abstract; column 5, lines 19-47; column 7, lines 8-31; claims 1-20 and figure 1-6 and 10) | 1- 4 and 8-11 |
| A | PHAN H.V et al. "Vibrating membrane with discontinuities for rapid and efficient microfluidic mixing" Lab Chip. 9 September 2015; Vol. 15(21), Pages 4206-16.<br>Abstract | 1-16 |
| A | US 6719449 B1 (LAUGHARN, Jr. et al.) 13 April 2004<br>Abstract, claims 1-6 and figures 1-9 | 1-16 |

| INTERNATIONAL SEARCH REPORT<br>Information on patent family members | International application No.<br>**PCT/AU2016/000299** |
|---|---|

This Annex lists known patent family members relating to the patent documents cited in the above-mentioned international search report. The Australian Patent Office is in no way liable for these particulars which are merely given for the purpose of information.

| Patent Document/s Cited in Search Report | | Patent Family Member/s | |
|---|---|---|---|
| **Publication Number** | **Publication Date** | **Publication Number** | **Publication Date** |
| WO 2009/122340 A1 | 08 October 2009 | WO 2009122340 A1 | 08 Oct 2009 |
| US 8240907 B2 | 14 August 2012 | US 2008247264 A1 | 09 Oct 2008 |
| | | US 8240907 B2 | 14 Aug 2012 |
| | | CN 101305277 A | 12 Nov 2008 |
| | | CN 101305277 B | 27 Mar 2013 |
| | | DE 102005043034 A1 | 15 Mar 2007 |
| | | EP 1922542 A1 | 21 May 2008 |
| | | EP 1922542 B1 | 30 Mar 2016 |
| | | WO 2007028820 A1 | 15 Mar 2007 |
| US 6719449 B1 | 13 April 2004 | US 6719449 B1 | 13 Apr 2004 |
| | | AU 1600000 A | 15 May 2000 |
| | | AU 5092901 A | 03 Oct 2001 |
| | | CA 2402985 A1 | 27 Sep 2001 |
| | | EP 1125121 A1 | 22 Aug 2001 |
| | | EP 1125121 B1 | 12 Dec 2007 |
| | | EP 1875960 A2 | 09 Jan 2008 |
| | | US 2002009015 A1 | 24 Jan 2002 |
| | | US 6948843 B2 | 27 Sep 2005 |
| | | US 2005150830 A1 | 14 Jul 2005 |
| | | US 7329039 B2 | 12 Feb 2008 |
| | | US 2004264293 A1 | 30 Dec 2004 |
| | | US 7521023 B2 | 21 Apr 2009 |
| | | US 2006029525 A1 | 09 Feb 2006 |
| | | US 7686500 B2 | 30 Mar 2010 |
| | | US 2008050289 A1 | 28 Feb 2008 |
| | | US 7687026 B2 | 30 Mar 2010 |
| | | US 2006158956 A1 | 20 Jul 2006 |
| | | US 7687039 B2 | 30 Mar 2010 |
| | | US 2010011845 A1 | 21 Jan 2010 |
| | | US 7811525 B2 | 12 Oct 2010 |
| | | US 2010124142 A1 | 20 May 2010 |
| | | US 7981368 B2 | 19 Jul 2011 |
| | | US 2008056960 A1 | 06 Mar 2008 |

Due to data integration issues this family listing may not include 10 digit Australian applications filed since May 2001.

| INTERNATIONAL SEARCH REPORT<br>Information on patent family members | International application No.<br>**PCT/AU2016/000299** |
|---|---|

This Annex lists known patent family members relating to the patent documents cited in the above-mentioned international search report. The Australian Patent Office is in no way liable for these particulars which are merely given for the purpose of information.

| Patent Document/s Cited in Search Report | | Patent Family Member/s | |
|---|---|---|---|
| **Publication Number** | **Publication Date** | **Publication Number** | **Publication Date** |
| | | US 8263005 B2 | 11 Sep 2012 |
| | | WO 0025125 A1 | 04 May 2000 |
| | | WO 0170381 A2 | 27 Sep 2001 |

**End of Annex**

Due to data integration issues this family listing may not include 10 digit Australian applications filed since May 2001.